The Journal of Experimental Biology 200, 3141–3164 (1997)
Printed in Great Britain © The Company of Biologists Limited 1997
JEB1287

FLOW AND FLEXIBILITY

I. EFFECTS OF SIZE, SHAPE AND STIFFNESS IN DETERMINING WAVE FORCES ON THE STIPITATE KELPS *EISENIA ARBOREA* AND *PTERYGOPHORA CALIFORNICA*

BRIAN GAYLORD* AND MARK W. DENNY

Hopkins Marine Station of Stanford University, Department of Biological Sciences, Pacific Grove, CA 93950, USA

Accepted 2 October 1997

Summary

Wave action on exposed rocky coasts can be severe, generating large hydrodynamic forces that have been proposed to constrain the size of intertidal animals and plants. In contrast, flows subtidally are more benign, and organisms, particularly seaweeds, may grow quite large. The large dimensions of these flexible macroalgae allow them to move during much or most of a passing wave cycle, reducing relative water velocities and modifying the forces the plants must endure. The consequences of such wave-induced motion are explored for the stipitate understory kelps *Eisenia arborea* and *Pterygophora californica* using a numerical model that approximates these seaweeds as vertically oriented cantilever beams subjected to lateral hydrodynamic forces acting at their stipe tips. Bending moments and peak stresses induced in the stipes of these species during the passage of waves are calculated as functions of plant size and shape and of water depth and sea state. Model predictions for a subset of conditions are validated against real-time measurements of bending moments acting on a *Pterygophora* individual in the field. The results suggest that the allometric patterns of growth exhibited by *Eisenia* and *Pterygophora* can greatly reduce the stresses generated in the stipes of these plants relative to isometric growth. Low stipe stiffness acts as a general, particularly effective, stress-lowering mechanism. The dynamic swaying associated with this low stiffness can also modulate the magnitudes of peak stresses induced in the stipes of these kelps. In particular, in shallow water under large waves, dynamic loading can substantially increase induced stress, suggesting that plant motion is an important factor affecting the loading regime encountered by these organisms.

Key words: kelp, *Eisenia arborea*, *Pterygophora californica*, wave action, hydrodynamic forces, nearshore ecology.

Introduction

Seaweeds live in habitats characterized by continuous, time-varying water motion. In the intertidal zone, organisms must cope with the violent flows produced by breaking waves. To survive the resulting large hydrodynamic forces imposed on them, plants and animals have evolved a variety of strategies that allow them to mediate the potentially destructive effects of their physical environment (for reviews, see Denny *et al.* 1985; Koehl, 1986). For example, many organisms take advantage of microhabitats protected from the full brunt of incoming waves (Emson and Faller-Fritsch, 1976; Koehl, 1977; Menge, 1978). Alternatively, animals such as barnacles and mussels thrive in fully exposed sites (Ricketts *et al.* 1985), but produce rigid tests or shells and strong adhesives (Murdock and Currey, 1978; Gubbay, 1983; Yule and Walker, 1987) or attach *via* flexible threads that deform into efficient safety harnesses when impacted by waves (Bell and Gosline, 1996). Indeed, 'strong and rigid' *versus* 'flexible and extensible' appear to be two dissimilar but equally effective themes in intertidal life (Koehl, 1984). Marine macroalgae conform to the latter category. When exposed to high-velocity flows or rapid accelerations, intertidal plants quickly reorient to become aligned with the direction of fluid motion and then reconfigure to an even more streamlined posture (Carrington, 1990). This reduces the plant area presented perpendicular to the oncoming flow and effectively lowers the drag imposed on an algal thallus. In contrast, forces that result from the water's acceleration past a plant are more effectively minimized by small overall size, since hydrodynamic accelerational forces increase with the volume of the organism rather than scaling with area. Denny *et al.* (1985) have proposed that this feature imposes constraints on the maximal size of intertidal animals that grow isometrically, and Gaylord *et al.* (1994) have extended this argument to intertidal macroalgae that change shape with growth.

In contrast to the intertidal zone, subtidal habitats are characterized by much less violent water motion. Concomitant with this reduction in hydrodynamic severity are organisms

*Author for correspondence: present address: Ecology, Evolution and Marine Biology, University of California, Santa Barbara, California 93106, USA (e-mail: bri@icess.ucsb.edu).

that are often quite large. *Macrocystis pyrifera*, the giant kelp, and *Nereocystis luetkeana*, the bull kelp, extend from depths of 30 m or more to the surface and may produce numerous blades that together comprise a total area of several to many square meters (Abbott and Hollenberg, 1976; Johnson and Koehl, 1994; Denny *et al.* 1997). Below the surface canopy of these species are often stipitate understory kelps such as *Eisenia arborea* and *Pterygophora californica*, erect seaweeds that can reach lengths in excess of 3 m from holdfast to blade tip (Abbott and Hollenberg, 1976).

Unlike small intertidal macroalgae, which quickly reorient with the initial impact of a wave and then remain extended and aligned with flow during its subsequent passage, the longer subtidal kelps can continue to move over a much larger fraction of any wave cycle before reaching the limits set by the length of their stipes or thalli. This interaction between the kinematics of the plant and the motion of the water itself can affect the stresses that may be generated within the tissues of these organisms. Indeed, Koehl (1982, 1984, 1986) has proposed that the flexibility of large macroalgae allows them to reduce drag by decreasing water velocities relative to their fronds.

In the present study, we explore potential consequences of plant flexibility in more detail, focusing on the mechanics of the interaction of time-varying flows with the stipitate subtidal kelps *Eisenia arborea* and *Pterygophora californica*. Each of these seaweeds is characterized by a single stiff, upright stipe that protrudes vertically upwards from a sturdy holdfast, with multiple blades borne near the tip of the stipe. *Eisenia* bears perennial thalli that extend from a distinctive, dichotomously branched and flattened distal portion of the stipe (Fig. 1A), while the stipe of *Pterygophora* is woody and remains unbranched, supporting a single terminal blade and numerous lateral sporophylls that emerge from the margins of a markedly flattened stipe terminus (Fig. 1B). Larger individuals of both species can possess 30–40 blades and sporophylls, some in excess of 1 m long, commonly 4–10 cm wide. The stipes themselves can reach 2 m in length with a diameter of 4 cm. The erect but flexible structure of both species allows them to sway under passing waves as water interacts with the thalli attached to the end of their stipes.

We approach an improved understanding of the dynamic behavior of *Eisenia* and *Pterygophora* in flow through the use of a simple numerical model that approximates these plants as vertically oriented cantilever beams subjected to horizontal hydrodynamic loads acting at their free ends and tracks their motion in response to waves. We first validate the model by checking its predictions against measurements of bending moments acting on the stipe of a *Pterygophora* individual exposed to wave-driven flows in the field. Once verified, the numerical model is used to explore the roles of seaweed size and shape, stipe material properties and plant motion in determining the bending moments and stresses acting on these kelps across a range of wave conditions and water depths.

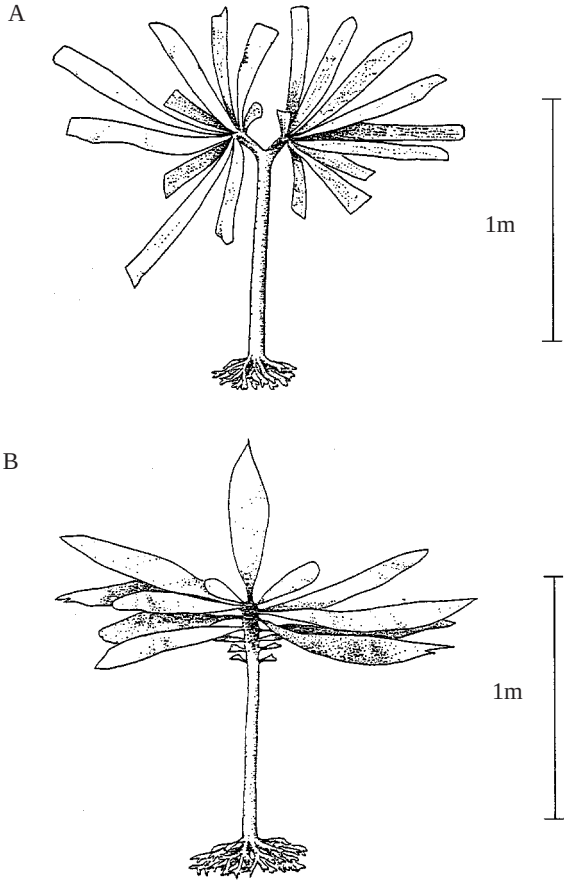

Fig. 1. (A) *Eisenia arborea*. (B) *Pterygophora californica*. For clarity, the seaweeds are shown in a fully splayed configuration; in nature, however, these plants reorient with flow.

Beam bending theory

Symbols are defined in Table 1.

The differential equation describing the behavior of a beam subjected to a dominant lateral or bending load is (Gere and Timoshenko, 1990):

$$M = -\kappa EI\ , \tag{1}$$

where M is the bending moment induced at the cross section of interest (cut in a plane perpendicular to the long axis of the beam), E is the beam's elastic modulus, I is the moment of inertia of the cross section about the neutral axis (the line corresponding to the infinitesimally thin layer within a beam that acts as the interface between the tensile and compressive regions and therefore undergoes no deformation during bending), and κ is the radius of curvature of the bent beam.

Calculus yields the equation for curvature (in standard X,Y coordinates, with the axis of the undeformed beam lying along the X-axis):

$$\kappa = \frac{\dfrac{d^2Y}{dX^2}}{\left[1+\left(\dfrac{dY}{dX}\right)^2\right]^{3/2}}\ . \tag{2}$$

Table 1. *Symbols*

Symbol		Equation where first used
A	Maximal projected area	13
A_c	Compressive area of the cross section of a bent beam	A1
A_t	Tensile area of the cross section of a bent beam	A1
C_a	Added mass coefficient	15
d	Water depth	16
e_f	Mean fractional error	24
E	Modulus (material stiffness)	1
E_c	Compressive modulus	9
E_t	Tensile modulus	9
E'	Altered modulus	–
E_c'	Altered compressive modulus	–
E_t'	Altered tensile modulus	–
$\hat{E}$	Reference modulus	–
$(EI)_{eff}$	Effective flexural stiffness of a beam when $E_t \neq E_c$	9
F	Lateral force applied to a beam	3
F_{am}	Added mass force	15
F_d	Drag	13
F_r	Restoring force	18
F_{vb}	Virtual buoyancy	14
$G_1(p)$	Complete elliptic integral of the first kind	8
$G_1(p,\Phi)$	Incomplete elliptic integral of the first kind	8
$G_2(p)$	Complete elliptic integral of the second kind	6
$G_2(p,\Phi)$	Incomplete elliptic integral of the second kind	6
$\boldsymbol{g}$	Acceleration due to gravity	17
H	Wave height	16
I	Moment of inertia of a beam cross section	1
I_c	Moment of inertia of the compressive portion of a beam cross section about the neutral axis	9
I_t	Moment of inertia of the tensile portion of a beam cross-section about the neutral axis	9
$\hat{I}$	Moment of inertia of a beam cross section computed about its centroidal axis	12
k	Wave number, $2\pi/\lambda$	16
L	Stipe or beam length	3
M	Bending moment	1
M_{obs}	Observed maximum bending moment	24
M_{pred}	Predicted maximum bending moment	24
M'	Bending moment resulting from altered moduli	–
$\hat{M}$	Bending moment resulting from the situation where moduli are equal	26
m	Total equivalent mass	18
p	Elliptic integral modulus	6
r	Stipe or beam radius	12
r_1	Stipe semi-axis perpendicular to the plane of bending	A4
r_2	Stipe semi-axis in the plane of bending	A4
s	Distance upwards from the substratum	16
SEE	Standard error of the regression estimate	–
S_d	Shape coefficient of drag	13
t	Time	14
u	Velocity of fluid relative to the substratum	14
u_x	Horizontal water velocity	16
u_r	Relative water velocity	13
u_{xr}	Horizontal relative water velocity	19
V	Volume of an organism	14
X	Position along horizontal axis in standard Cartesian coordinate system	2
x	Horizontal displacement or position	16
Y	Position along vertical axis in standard Cartesian coordinate system	2
$\bar{y}$	Perpendicular distance from the neutral axis in the plane of the cross section	A2
$\bar{y}_c$	Perpendicular distance from the neutral axis to the compressive surface of the stipe in the plane of the cross section	11
$\bar{y}_t$	Perpendicular distance from the neutral surface to the tensile surface of the stipe in the plane of the cross section	10
y_n	Distance of the neutral axis from the centroidal axis of the stipe	A5
α	Coefficient in the allometric equation	22
β	Exponent in the allometric equation	22
γ	Component of the velocity exponent in the drag equation	13
δ_{axl}	Deflection of the tip of a beam parallel to its undeformed long axis	5
δ_{lat}	Deflection of the tip of a beam perpendicular to its undeformed long axis	4
Φ	Elliptic integral amplitude	6
κ	Beam curvature	1
λ	Wavelength	17
ρ	Mass density of a fluid	13
σ	Stress	–
σ'	Altered stress, tensile or compressive	–
$\hat{\sigma}$	Stress with both moduli equal	12
σ_c	Compressive stress	11
σ_t	Tensile stress	10
τ	Wave period	16
ω	Wave frequency, $2\pi/\tau$	16
ζ	Zero offset in allometric tensile modulus curve fits	23
ψ	Substitution variable for integration	–

For a very stiff beam and small lateral tip load (F), the end of the beam deflects only slightly; thus, the slope of the beam (dY/dX) is small and κ approximates to d^2Y/dX^2. Under these conditions, M is very nearly just the product of the force times the distance from the end of the undeformed beam to the cross section of interest (at X). Thus, for small deflections, equation 1 simplifies to:

$$F(L-X) = -\frac{d^2Y}{dX^2}EI\ , \tag{3}$$

where L is the length of the beam. Upon integration and application of the appropriate boundary conditions, this yields the well-known linear approximations for tip deflection:

$$\delta_{lat} = \frac{FL^3}{3EI}\ , \tag{4}$$

$$\delta_{axl} = 0\ , \tag{5}$$

where δ_{lat} is the deflection of the tip of a beam perpendicular to its undeformed long axis and δ_{axl} is the deflection parallel to this axis. These quantities are defined in Fig. 2A.

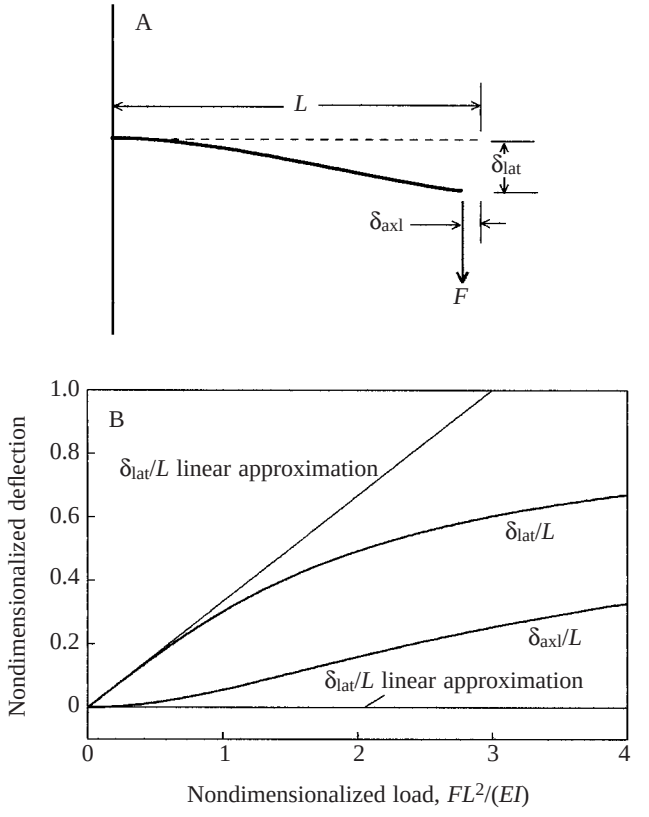

Fig. 2. (A) Geometry of a bent beam. (B) Comparison of tip deflections from simplified linear beam bending theory (equations 4, 5) with the large-deflection, nonlinear theory (equations 6, 7). L, beam length; F, lateral load applied to beam; δ_{lat}, deflection of the beam tip perpendicular to its undeformed long axis; δ_{axl}, deflection of the beam tip parallel to its undeformed long axis; E, elastic modulus; I, moment of inertia of beam cross section.

Equation 4 and 5, however, are acceptable only for small deflections ($\delta_{lat}<L/10$). For more extreme deflections (such as those experienced by stipitate kelps), the linear theory becomes increasingly inaccurate owing to the increase in slope and reduction in moment arm as the beam bends, and equation 1 must be solved using the exact expression for curvature. For a concentrated lateral load applied to the end of a cantilever beam, an analytical solution exists in the form of elliptic integrals (Charters *et al.* 1969; Gere and Timoshenko, 1990):

$$\delta_{lat} = L\left\{1 - \sqrt{\frac{4EI}{FL^2}}\left[G_2(p) - G_2(p,\Phi)\right]\right\}, \tag{6}$$

$$\delta_{axl} = L\left\{1 - \sqrt{\frac{2EI(2p^2-1)}{FL^2}}\right\}. \tag{7}$$

where $G_2(p)$ and $G_2(p,\Phi)$ are the complete and incomplete elliptic integrals of the second kind, respectively. p is the elliptic integral modulus and Φ is the elliptic integral amplitude (Abramowitz and Stegun, 1965), quantities related to the bent geometry of a beam *via* the expression (Gere and Timoshenko, 1990):

$$G_1(p) - G_1(p,\Phi) = \sqrt{\frac{FL^2}{EI}}\ , \tag{8}$$

where $G_1(p)$ and $G_1(p,\Phi)$ are the complete and incomplete elliptical integrals of the first kind (again with modulus p and amplitude Φ), respectively, and $FL^2/(EI)$ represents the nondimensionalized lateral load which determines the deflection curve of the beam (and thus p and Φ). The relationships of equation 6 and 7 are plotted in Fig. 2B for comparison with the simplified linear theory. We also note that, although elliptic functions may be unfamiliar to many biologists, they should not be viewed as arcane; indeed G_1 and G_2 may be computed numerically or interpolated from published tables in much the same way that one would find the sine or cosine of a particular angle if an electronic calculator were unavailable.

Unequal moduli

Some materials are not equally stiff in tension and compression (i.e. the tensile modulus, E_t, does not equal the compressive modulus, E_c). Under these conditions, EI is replaced by an effective flexural stiffness $(EI)_{eff}$ (Gere and Timoshenko, 1990), defined by:

$$(EI)_{eff} = E_tI_t + E_cI_c\ , \tag{9}$$

where I_t and I_c are the moments of inertia of the tensile and compressive regions of the beam cross section, respectively, computed about the neutral axis. Note that, owing to the difference in tensile and compressive moduli, the neutral axis no longer passes through the geometric center (i.e. the centroid) of the beam cross section (see Appendix).

The maximum stresses at a given cross section within the tensile portion of a bent beam are then given by:

$$\sigma_t = \frac{M\bar{y}_t E_t}{(EI)_{eff}} , \quad (10)$$

while those in the compressive region are given by:

$$\sigma_c = \frac{M\bar{y}_c E_c}{(EI)_{eff}} , \quad (11)$$

where $\bar{y}_t$ and $\bar{y}_c$ are the perpendicular distances from the neutral axis of the beam cross section to the tensile or compressive surfaces of the beam, respectively. Note that for E_t=E_c, these equations reduce to the standard bending stress formula for isotropic, homogeneous materials (Wainwright *et al.* 1976; Denny, 1988):

$$\hat{\sigma} = \frac{Mr}{\hat{I}} , \quad (12)$$

where $\hat{\sigma}$ is the maximum stress induced at a given beam cross section, r is the radius of the beam and $\hat{I}$ is the moment of inertia computed about the beam's centroidal axis.

A simple numerical model of the mechanics of cantilever kelps

The consequences to *Eisenia* and *Pterygophora* of time-dependent fluid forces can be explored in a rudimentary fashion through the analysis of the dynamics of bending beams *via* an extension of the theory developed above. The major components in this model are described below.

Total equivalent mass

The total moving mass of a stipitate kelp consists of its blade mass (which can be approximated as a point mass located at the stipe terminus) plus the distributed mass of the stipe. The dynamic effects of the stipe's distributed mass can be modeled equivalently by a lumped 'effective' mass, located at the stipe tip. For a stipe of constant cross section, this effective mass equals 24 % of the stipe mass (Thomson, 1993). Thus, the sum of the blade mass plus 24 % of the stipe mass provides an estimate of the total equivalent plant mass, which is viewed as being positioned at the end of the stipe.

Fluid forces

The blades of *Eisenia* and *Pterygophora* grow from the distal region of their stipes and are responsible for most of the hydrodynamic forces imposed on the total equivalent mass. These forces act predominantly along a horizontal axis and can therefore be modeled (in analogy to a cantilever beam) as lateral loads applied to the stipe tip. Three major fluid-dynamic forces are present.

Drag (F_d): water motion relative to an alga tends to push it downstream (Denny, 1995):

$$F_d = \tfrac{1}{2}\rho A S_d u_r^{\gamma} , \quad (13)$$

where ρ is the mass density of the fluid, A is a representative area, S_d is the shape coefficient of drag with dimensions $m^{2-\gamma}s^{\gamma-2}$, u_r is the fluid's velocity relative to the organism and γ is the velocity exponent.

Virtual buoyancy (F_{vb}): when the velocity of fluid particles within a flow change with time, the pressure gradient associated with such an accelerating flow imposes an additional force in the direction of fluid acceleration (Batchelor, 1967):

$$F_{vb} = \rho V \frac{du}{dt} , \quad (14)$$

where du/dt is the acceleration of the fluid relative to the substratum and V is the volume of the organism.

Added mass force (F_{am}): a third force is produced if fluid accelerates relative to an organism (Batchelor, 1967):

$$F_{am} = C_a \rho V \frac{du_r}{dt} , \quad (15)$$

where C_a is the nondimensional added mass coefficient (Batchelor, 1967; Daniel, 1984) and du_r/dt is the acceleration of the fluid relative to the organism. F_{am} acts in the direction of relative acceleration.

Water motion under waves

Horizontal water velocities (u_x) under nonbreaking waves are described accurately by linear wave theory (Kinsman, 1965; Denny, 1988):

$$u_x = \frac{\pi H}{\tau} \cos(kx - \omega t) \frac{\cosh(ks)}{\sinh(kd)} , \quad (16)$$

where H is wave height, τ is wave period, k is the wave number ($2\pi/\lambda$, where λ is the wavelength), ω is the radian wave frequency ($2\pi/\tau$), x is horizontal position, d is water depth, s is the distance above the bottom, and t is time; sinh and cosh are the hyperbolic sine and cosine functions, respectively. Note that λ, d and τ are not independent; a simple approximation of their relationship is given by Eckart (1952):

$$\lambda \cong \frac{\boldsymbol{g}\tau^2}{2\pi} \sqrt{\tanh\left(\frac{4\pi^2 d}{\tau^2 \boldsymbol{g}}\right)} , \quad (17)$$

where $\boldsymbol{g}$ is the acceleration due to gravity and tanh is the hyperbolic tangent. Equation 16 (and its temporal derivative) provides estimates of the horizontal velocities and accelerations leading to the dominant drag, virtual buoyancy and added mass forces acting on the kelps.

Restoring force

The fluid forces imposed by wave-driven water motion are in turn resisted by the internal stiffness of a kelp's stipe. In bending theory, a particular nondimensionalized cantilever lateral load is associated with a given static nondimensionalized deflection (Fig. 2B). Thus, the *restoring*

force (F_r) of a stipe bent to a given deflection equals the negative of the force required to achieve that same deflection under conditions of static equilibrium. This relationship is described by equation 8 (with F_r=F), where p and Φ are set by the deflection geometry determined by equations 6 and 7.

Force balance

From Newton's Second Law, any instantaneous imbalance between the applied fluid forces and internal stipe stiffness results in lateral acceleration of the total equivalent mass:

$$m\frac{\mathrm{d}^2x}{\mathrm{d}t^2} = F_\mathrm{d} + F_\mathrm{vb} + F_\mathrm{am} - F_\mathrm{r}\ , \qquad (18)$$

where x represents the lateral deflection of the tip of the stipe, and m is the total equivalent plant mass located at the end of the stipe.

Substituting from equations 8 and 13–15 yields:

$$m\frac{\mathrm{d}^2x}{\mathrm{d}t^2} = \tfrac{1}{2}\rho A S_\mathrm{d}\, u_\mathrm{xr}\left|u_\mathrm{xr}\right|^{\gamma-1} + \rho V\frac{\mathrm{D}u_\mathrm{x}}{\mathrm{D}t} + C_\mathrm{a}\,\rho V\left(\frac{\mathrm{D}u_\mathrm{x}}{\mathrm{D}t} - \frac{\mathrm{d}^2x}{\mathrm{d}t^2}\right) - \left[G_1(p) - G_1(p,\Phi)\right]^2\frac{(EI)_\mathrm{eff}}{L^2}\ , \qquad (19)$$

where u_xr is the horizontal relative water velocity:

$$u_\mathrm{xr} = u_\mathrm{x} - \frac{\mathrm{d}x}{\mathrm{d}t}\ , \qquad (20)$$

and where:

$$\frac{\mathrm{D}u_\mathrm{x}}{\mathrm{D}t} = \frac{\partial u_\mathrm{x}}{\partial t} + u_\mathrm{x}\frac{\partial u_\mathrm{x}}{\partial x}\ . \qquad (21)$$

The inclusion of $\mathrm{D}u_\mathrm{x}/\mathrm{D}t$, the 'total' or 'substantive derivative', accounts for the dependence of u_x on both time and space. In the numerical implementation used in this study, only the horizontal component of water motion (and thus applied force) is included. Note that, in shallow water, horizontal velocities are much greater than vertical velocities (Kinsman, 1965; Denny, 1988); thus, this simplification is justified.

Equation 19 is not amenable to analytical solution. As an alternative, a fourth-order Runge–Kutta numerical algorithm is used (Press *et al.* 1992). The choice of initial conditions is arbitrary (for t greater than one full wave period) owing to substantial hydrodynamic damping. The elliptic integral term in equation 19 is found by interpolating from a large 'look-up table' computed using *Mathematica* (Wolfram Research) and stored in the computer memory.

The solution of equation 19 yields a description of the motion of the total equivalent mass (i.e. the stipe tip) through time. Since the stress induced in a stipe of given geometry and elastic modulus is a direct function of tip deflection [δ_lat and M in equations 10 and 11 are coupled *via* the elliptic integrals of equations 6–8, where M=$F(L-\delta_\mathrm{axl})$], this description of the plant's movement also determines the maximum bending moments imposed and the maximum stresses generated in the stipe.

Materials and methods

Allometry

Eisenia arborea Areschoug and *Pterygophora californica* Ruprecht were collected using SCUBA in Carmel Bay (Carmel-by-the-Sea, California) on the Monterey Peninsula in central California from between 15 and 25 m of water during May and June 1994 and were stored in running sea water until experiments were completed (always within 72 h of collection).

For each individual collected, measurements were made of stipe length, stipe radius along orthogonal axes at both the base and stipe tip, stipe mass, blade mass and the total projected blade area. Thirty-three individuals of *Eisenia* and 37 *Pterygophora* were examined, across a wide range of sizes. Total projected blade area (A in equation 13) was determined by laying all the blades from a plant on a piece of paper, tracing them, and then comparing the mass of the tracing with the mass of a piece of paper of known area. Blade volume, V, was computed by dividing the blade mass by 1050 kg m^{-3}, a typical density for algal materials.

Data were expressed as functions of stipe length, L (used as an index of size), and fitted using standard ordinary least-squares (OLS) linear regressions to the $\log_e$-tranformed data (due to heteroscedasticity; Zar, 1974). This procedure yielded curve fits with a power law form:

$$\text{trait of interest} = \alpha L^\beta\ . \qquad (22)$$

α was multiplied by $e^{SEE^2/2}$, the standard correction factor used to account for the bias introduced by $\log_e$-transformation (Sprugel, 1983). *SEE* denotes the standard error of the regression estimate.

Moduli

The material stiffnesses in tension and compression of *Eisenia* and *Pterygophora* (and two other species of laminarian kelps, *Laminaria setchellii* and *Pleurophycus gardneri*) were evaluated in a two-step process. First, the ratio of tensile modulus to compressive modulus was estimated by measuring the shift away from the centroid of the location of the neutral axis of the stipe. Second, the effective flexural stiffness, $(EI)_\mathrm{eff}$, was found by using a simple cantilever linear beam bending test. E_t and E_c were then calculated from these data.

The off-center location of the neutral axis was determined as follows. Several 10 cm long, 20 gauge hypodermic needles were driven through the center of a straight and uniform section of algal stipe, perpendicular to the long axis of the stipe and parallel to one another. The stipe, oriented horizontally with needles protruding from the top and bottom, was then photographed in an unbent posture and under two different levels of vertical bending. The camera was equipped with a telephoto lens and positioned approximately 7 m distant to minimize parallax. Bending the stipe caused the needles to

rotate relative to one another (splaying apart on the tensile side of the stipe and converging on the compressive side). The arc lengths between each pair of adjacent needles were then measured by projecting the photographs of stipe and needle position onto a digitizing pad, and the location within the stipe where the arc lengths remained equal under both the bent and unbent conditions (i.e. the location of the neutral axis) was noted. The degree of shift of the neutral axis away from the center of the stipe cross section provides a quantitative estimate of the ratio E_t/E_c (see Discussion and Fig. 12).

The mean value of E_t/E_c for each species was then used in conjunction with a simple linear cantilever test to estimate the tensile and compressive moduli of the plants. A straight section of stipe of uniform cross section was clamped at one end in a horizontal orientation. Weights were hung from the free end and the vertical deflection at the tip, δ_{lat}, was recorded. In no instance did the deflection exceed 10 % of the length of the cantilevered sample. The effective flexural stiffness of the stipe was estimated from equation 4, with F set equal to the weight hung from the end of the stipe. The weight of the stipe itself was neglected. A given value of E_t/E_c also sets the ratio $(EI)_{eff}/(E_t\hat{I})$ (see Discussion and Fig. 12), where $\hat{I}$ is again the moment of inertia computed about the centroidal axis of the cross section. Thus, E_t was estimated by dividing the measured value of $(EI)_{eff}$ by the product of $\hat{I}$ and the value of $(EI)_{eff}/(E_t\hat{I})$ predicted on the basis of E_t/E_c for that species (see Table 4). Once E_t had been found, the compressive modulus was calculated by dividing E_t by the appropriate E_t/E_c value. Tensile and compressive moduli were estimated for each sampled plant, when possible, across the full range of sizes. Occasionally, stipe irregularities, excessive curvature or taper, or damage from grazers prevented measurement of the flexural stiffness (and thus the moduli). Tensile modulus for each species was expressed as a function of stipe length:

$$E_t = \alpha L^{\beta} + \zeta, \qquad (23)$$

with ζ set equal to the minimum measured tensile modulus of that species. The zero offset, ζ, was included since the stiffness of a plant does not drop to zero even in exceptionally small individuals. The fit to equation 23 was calculated by first subtracting ζ and then performing an OLS regression on the $\log_e$-transformed residuals as described above. E_c was also expressed as a function of L by dividing equation 23 by the E_t/E_c ratio of that species.

Determination of drag and added mass coefficients

Drag coefficients for *Eisenia* and *Pterygophora* were measured for single individuals of each species using the boat-mounted apparatus of Utter and Denny (1996) modified to include a cantilever-style force transducer for improved accuracy. S_d and γ in equation 13 were computed by fitting the resulting untransformed velocity–force data with a nonlinear least-squares curve-fitting routine (Press *et al.* 1992).

Although the large size of *Eisenia* and *Pterygophora* makes determination of their added mass coefficients difficult, we were able to measure as an alternative the C_a of *Pleurophycus gardneri*, a smaller, related laminarian kelp that also has a stipitate form. The 'tow tank' apparatus used is described in Denny and Gaylord (1996). Although *Pleurophycus* has only a single blade, its erect stipe and general structure are reminiscent of those of *Eisenia* and *Pterygophora*, and it is likely that the added mass coefficients of these three species are quite similar. This substitution is also of little consequence owing to the slow fluid accelerations characteristic of subtidal habitats.

Field experiments

The apparatus shown in Fig. 3 was used to record the bending moments imposed at the base of the stipe on a *Pterygophora* individual exposed to waves in the field. The plant was strapped securely *via* its holdfast to a baseplate, which in turn was bolted rigidly to a torque-measuring transducer. This positioned the seaweed on the device much as it would grow in nature from a flat substratum. The torque transducer proper consisted of a thin-walled, hollow cylinder, oriented horizontally with one end fixed to a rigid support frame. Strain gauges mounted on the outside of the cylinder sensed any torsion of the cylinder resulting from bending moments applied to the attached plant. The voltage ouput from the transducer (which increases linearly with bending moment) was amplified and sampled at 20 Hz by a digital datalogger (Tattletale model 5F). The datalogger also simultaneously recorded the output from a pressure transducer (Omega PX176A) which measured the depth of the water above the apparatus.

The torque transducer and attached plant were deployed using SCUBA for 1 h on 10 October 1996 in approximately 3.5 m of water. This location was nominally just outside the breaker line; thus, the waves were actively shoaling by the time

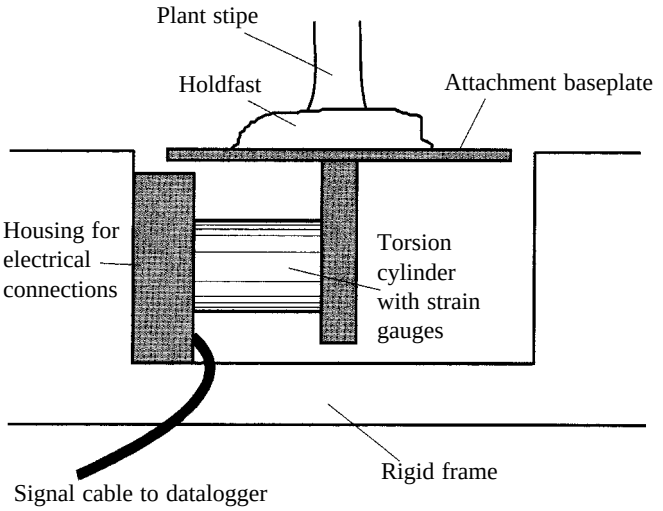

Fig. 3. Field torque transducer. Strain gauges mounted on the torsion cylinder at 45 ° relative to its axis sense bending moments acting in a plane perpendicular to the page. The recorded bending moments were corrected for the small vertical offset of the plant above the center of rotation of the torsion cylinder.

Table 2. *Morphological characteristics of the* Pterygophora californica *individual tested in the field*

Stipe radius, r	0.008 m
Stipe mass, m	0.114 kg
Blade mass	0.221 kg
Blade area, A	0.301 m^2
Tensile modulus, E_t	205 MPa

they reached the vicinity of the apparatus and plant. The device was oriented to sense bending moments acting in the vertical plane aligned with the direction of wave propagation. The upper surface of the transducer support frame was positioned flush with the surrounding substratum, and a weight of 40 kg was used to hold the support frame immobile on the seabed. The site selected was flat, with a sandy substratum, and was located far (at least 30 m along the axis of wave propagation and 10 m parallel to the shoreline) from all rocks or reefs large enough to add topographical complexity. The waves arriving during the experiment were characterized by a significant wave height of 0.82 m and a dominant period of 12 s. The largest waves recorded during the experiment were approximately 1.3 m in height. Although these conditions are benign compared with those that occur during winter storms, they are near the limit at which the device can be safely deployed by divers.

For analysis, the data record from the field deployment was divided into consecutive 4096 point segments to facilitate processing, and the pressure measurements during each segment were corrected for depth attenuation using standard spectral methods (Kinsman, 1965; Denny, 1988). The resulting corrected sea surface records (which define flow conditions *via* equation 16) were used as input parameters in the numerical model, together with the morphological parameters of the *Pterygophora* individual placed in the field (Table 2). Solution of the model yielded predictions of bending moments through time, which were then compared with the actual moments measured on the plant. This procedure provided a field test of the ability of the computational model to describe accurately the effects of wave-driven water motion on a stipitate kelp.

The correspondence between model predictions and field measurements was quantified in two ways. First, the mean and standard deviation of the predicted and measured bending moments were compared. Second, the mean fractional error (e_f) of the wave-by-wave maximum bending moment was calculated as:

$$e_f = 2\,\frac{M_{obs} - M_{pred}}{M_{obs} - M_{pred}}\ , \qquad (24)$$

where M_{obs} is the measured maximum moment and M_{pred} is the predicted maximum moment; the sign of the maxima occurring in the negative (i.e. seaward) direction was converted to positive values for the purposes of the above calculation. The first 20 s of each record was excluded from this procedure to eliminate any bias associated with the initial equilibration of the numerical model.

Numerical experiments

Once validated, the numerical model was used to explore variations in maximum bending moment and maximum stress as a function of seven basic parameters.

Effects of plant size

Model plants were 'grown' from small (L=0.1 m) to large (L=2 m) size, with A, V, m, E_t, E_c and r (stipe radius) all expressed as functions of stipe length according to the allometric measurements for *Eisenia* and *Pterygophora* shown in Table 3. This size range spanned the algal sizes sampled and observed in the field.

Effects of water depth

The model organisms were 'grown' in different depths of water ranging from 3 to 18 m. These values encompass the subtidal depths where these species are commonly found.

Effects of wave height

Plant size was increased across the range L=0.1–2 m, at depths of 3–18 m, for each of three values of H: 2, 4 and 6 m. Note that surface waves are expected to break when H/d exceeds approximately 0.78, producing much more complicated flows. When this occurs, linear wave theory becomes invalid, and the model is inappropriate. Therefore, water depth was decreased only to 3 m for H=2 m and only to 6 m for the wave heights H=4 and 6 m. Roughly, the values H=2, 4 and 6 m correspond to the largest waves one might expect in a year for a very protected, moderately protected and lightly exposed location, respectively (Denny, 1995). The sites where these plants were collected correspond most closely to the middle category.

Effects of wave period

Wave period was varied from 4 to 20 s, for plants with stipe lengths of 0.5, 1.0 and 1.5 m. Water depth was fixed at 10 m (a typical depth where these organisms live), and wave height was set to 4 m (conditions characteristic of a fairly severe winter storm).

Effects of plant shape

The consequences of two modes of isometric growth (i.e. growth characterized by no change in shape with size) were explored. The first mode represents isometric growth with a 'small-plant' form (i.e. the curve the plant would follow if it were to continue growing from L=0.1 m without changing shape). The second mode represents the growth pattern a plant would have to follow if it were to grow, with a constant shape, to the dimensions it shows at a large size of L=2 m. The exact functions defining the two isometric growth modes are given in Table 3. Note that the observed changes in moduli with size were retained so as to focus exclusively on the effects of plant shape.

Effects of material stiffness

The consequences of having either more flexible or stiffer

Table 3. *The growth patterns in* Eisenia arborea *and* Pterygophora californica *and in the hypothetical plants used in the numerical experiments*

	Natural plants						Isometric 'small' plants		Isometric 'large' plants	
	α	β	ζ	*SEE*	*N*	*P* (β=0)	α	β	α	β
Eisenia arborea										
Stipe radius (m)	0.021	0.619	–	0.161	33	<0.001	0.100	1	0.032	1
Stipe mass (kg)	0.725	2.145	–	0.243	33	<0.001	5.193	3	0.401	3
Blade mass (kg)	0.393	1.407	–	0.550	33	<0.001	15.38	3	0.130	3
Blade area (m^2)	0.495	1.168	–	0.513	33	<0.001	3.364	2	0.278	2
Tensile modulus (MPa)	57.9	1.047	15.6	1.036	29	<0.002	Same as natural plants			
Pterygophora californica										
Stipe radius (m)	0.012	0.787	–	0.196	37	<0.001	0.040	1	0.021	1
Stipe mass (kg)	0.262	2.518	–	0.367	37	<0.001	0.795	3	0.188	3
Blade mass (kg)	0.512	1.627	–	0.809	37	<0.001	12.07	3	0.198	3
Blade area (m^2)	0.654	1.396	–	0.722	37	<0.001	2.628	2	0.430	2
Tensile modulus (MPa)	306	2.228	108	0.997	25	<0.001	Same as natural plants			

The coefficients α and β refer to the equation: trait of interest = αL^{β}. ζ is the zero offset in allometric tensile curve fits; *SEE* is the standard error of the regression estimate.

stipes were explored by either decreasing or increasing E_t and E_c by a factor of 10. Also, the effects of having unequal moduli in tension and compression were examined analytically, for static loadings, over a modulus ratio (E_t/E_c) ranging from 0.1 to 10.

Effects of plant motion

The model was used to test further how plant movement itself affects the stresses induced in the stipe. The peak hydrodynamic load was computed and the so-called 'static' stress that would result if it were applied as a constant, unvarying force was calculated. This static stress was then compared with the actual stress predicted by the model when the complete dynamic behavior of a flexible organism was considered. These comparisons were repeated for both species across the full size range and for all the depths and wave heights detailed above.

Results

Allometry

For both *Eisenia* and *Pterygophora*, stipe radius, stipe mass, blade mass and blade area all increased with increasing stipe length (Table 3). All morphological parameters, however, increased at a rate slower than that required for isometric growth (Student's *t*-test, $P<0.005$). Thus, the plants of these species of seaweed change shape with size, getting relatively more slender as they grow.

Stipe radius *versus* stipe length for both species increased with exponents less than 1 (Table 3). Thus, *Eisenia* and *Pterygophora* tend to produce stipes that, although thicker in an absolute sense, are proportionately more slender as the plants grow taller. Of the two species, *Eisenia* produces a thicker stipe, but *Pterygophora* shows a greater increase in stipe radius with increasing length.

Stipe mass increased with stipe length raised to an exponent of approximately 2 for both species. Given the relationships between stipe length and stipe radius, this is to be expected and suggests that the mass density of the stipe material remains more or less constant across size.

Blade mass increased at a similar rate for *Eisenia* and *Pterygophora*. At small stipe lengths, *Eisenia* has slightly more blade mass, while at large size *Pterygophora* has more frond material. In both cases, blade mass increased at a slower rate with stipe length than did stipe mass. These differences are significant ($P<0.001$). For both species, the allometric curve for blade mass deviated farthest from isometry of the four measured morphological parameters.

Blade area increased in a similar fashion to blade mass for both of the stipitate algae (the exponents of the blade mass and blade area regressions are not significantly different at $P<0.05$ for either of the species). This suggests that the blades of these species remain approximately the same thickness across size.

Moduli

All plants tested, including *Eisenia*, *Pterygophora*, *Laminaria* and *Pleurophycus*, exhibited shifts of their neutral axes away from the center of their stipes. Table 4 gives values of $(r-y_n)/r$ (where y_n is the perpendicular distance from the centroidal axis to the neutral axis of the stipe) and the corresponding ratios of tensile to compressive moduli. $(r-y_n)/r$ would equal 1 if the tensile and compressive moduli were the same. Estimates of E_t/E_c ranged from a maximum of over 8 for

Table 4. *Moduli ratios for four stipitate seaweeds*

	Sample	$\frac{r - y_n}{r}$	S.E.M.	N	$\frac{E_t}{E_c}$	$\frac{\bar{y_t}E_t}{\bar{y_c}E_c}$	$\frac{(EI)_{eff}}{E_t\hat{I}}$
Eisenia arborea	1	0.771	0.121	4	3.012	–	–
	2	0.746	0.120	10	3.403	–	–
	3	0.713	0.047	10	4.024	–	–
	4	0.856	0.022	10	1.985	–	–
	Mean	–	–	–	3.106	1.921	0.529
Laminaria setchelli	1	0.800	0.031	10	2.604	–	–
	2	0.728	0.099	10	3.731	–	–
	3	0.700	0.047	10	4.314	–	–
	4	0.726	0.117	10	3.767	–	–
	Mean	–	–	–	3.604	2.093	0.482
Pleurophycus gardneri	1	0.848	0.112	10	2.065	–	–
	2	0.751	0.087	10	3.315	–	–
	3	0.620	0.104	10	6.656	–	–
	4	0.732	0.136	5	3.660	–	–
	Mean	–	–	–	3.924	2.198	0.457
Pterygophora californica	1	0.820	0.082	9	2.355	–	–
	2	0.748	0.185	10	3.377	–	–
	3	0.577	0.072	10	8.457	–	–
	Mean	–	–	–	4.730	2.448	0.404

Abbreviations are defined in Table 1.

one *Pterygophora* stipe, to a mimimum of just below 2 for one of the *Eisenia* plants. In general, mean E_t/E_c values varied from approximately 3–4 among the species. For *Pterygophora*, the mean tensile to compressive modulus ratio was 4.7, close to the value of 4.2 reported by Biedka *et al.* (1987).

Both *Eisenia* and *Pterygophora* also showed evidence that their material properties change with growth (preliminary data for *Laminaria* and *Pleurophycus* show similar trends, but we have not included them here). The moduli of the stipes of both of these seaweeds increased with stipe length (Table 3). Such changes in material properties with growth are unusual, but have been observed in other biological systems as well (Katz and Gosline, 1994). *Eisenia* had substantially lower stiffness than *Pterygophora*; even the largest of these plants showed modulus values that were lower than those of juvenile *Pterygophora* specimens. The moduli of *Eisenia* also increased more slowly with stipe length than those of *Pterygophora*. The tensile modulus of the larger *Pterygophora* reached nearly 700 MPa, eight times that of the largest measured value for *Eisenia*. Smaller *Pterygophora* had tensile moduli of approximately 100 MPa. These values are somewhat greater than those found for two *Pterygophora californica* plants by Biedka *et al.* (1987), who measured tensile moduli of 45–60 MPa in extracted tissue samples and report a tensile modulus of 75 MPa for the intact stipe of a single juvenile plant. Unfortunately, the size of the specimens Biedka *et al.* (1987) used is unknown, as is the structural integrity of the tissue they measured, since they report that their specimens had been collected up to 3 weeks prior to testing.

Drag and added mass measurements

Velocity exponents were 1.55 for *Eisenia* and 1.23 for *Pterygophora*. S_d was 0.041 for *Eisenia* and 0.042 for *Pterygophora*. *Pleurophycus* had an added mass coefficient, C_a, of 1.77. These values are typical of those recorded in studies of other macroalgae (Gaylord *et al.* 1994).

Field experiments

Model predictions for the bending moments imposed at the base of the stipe on the *Pterygophora* individual tested in the field matched closely those recorded on the plant. Fig. 4A shows the high degree of overlap between the empirically measured bending moment distribution and the corresponding numerically predicted distribution. Both measured and predicted means are centered on zero, as one would expect from bidirectional loading produced by wave surge. The mean measured bending moment was 0.061±0.503 N m (mean ± S.D.). The mean predicted bending moment was 0.004±0.457 N m. Although these two means are significantly different (P<0.001 level, Student's t-test), the difference is small. The significance results primarily from the exceptionally large sample size (N=62 833).

The mean maximum bending moment measured for the 215 waves that arrived during the field test was 0.750±0.436 N m (N=430, with a positive and negative peak per wave). The mean maximum predicted bending moment was 0.717±0.307 N m. These means are not significantly different. The mean fractional error of the predicted maximum bending moments was −3.6 %.

A typical time trace of the measured and predicted bending

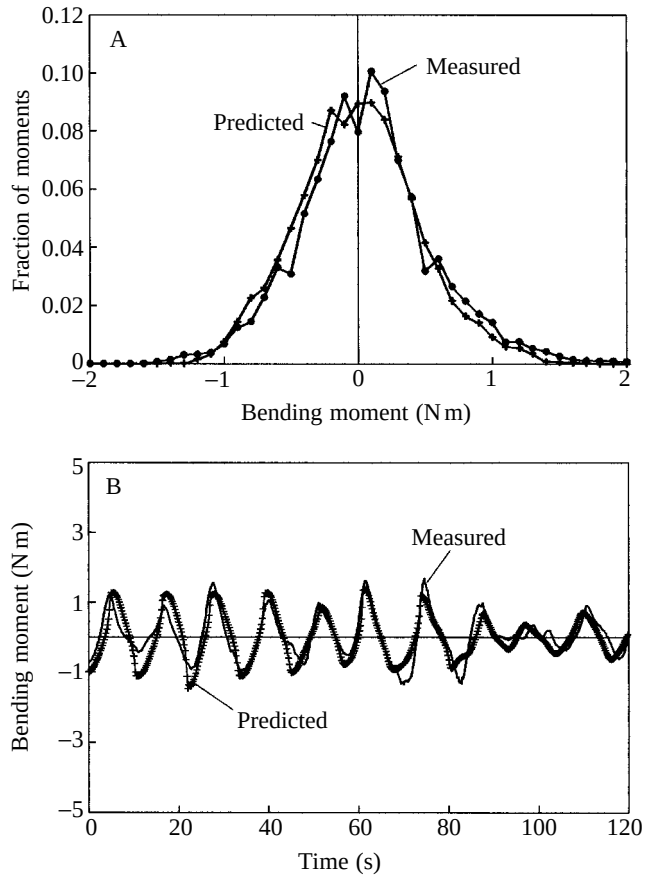

Fig. 4. (A) Comparison of the measured bending moment distribution acting on the *Pterygophora californica* individual tested in the field with that predicted by the numerical model. (B) Comparison of a typical recorded time series of the bending moment imposed on the stipe of the field-tested *Pterygophora* with that predicted by the numerical model.

moments acting at the base of the stipe on the field-tested *Pterygophora* is shown in Fig. 4B. In general, the predicted bending moments follow closely those actually measured, both in magnitude, as discussed above, and in time. The mean phase shift between the measured and predicted peaks was only 0.11±2.02 s (mean ± S.D., N=430). This mean phase shift was less than 1 % of the 12 s wave period of the swell arriving at the shore during the field trial.

Numerical experiments

The computer model predicts that the maximum bending moments and stresses (which occur at the base of the stipe) imposed on *Eisenia* and *Pterygophora* vary in a complex fashion with multiple wave and morphological parameters. These data are shown in Figs 5 and 6. With regard to the predictions of maximal stress, we present only tensile data, since maximum compressive stresses vary in an identical fashion to tensile stresses with each model parameter, but are simply lower by a fixed ratio (see Discussion). This ratio ($\overline{y}_t E_t / \overline{y}_t E_c$) is 1.92 for *Eisenia* and 2.45 for *Pterygophora* (Table 4).

Occasionally, for small plant sizes in shallow water, the seaweeds are predicted to deflect sufficiently far that the deflection curve approaches its asymptotic limit. Under these conditions, round-off error in the mathematical model prevents an accurate solution of the equation of motion. We therefore do not include data from these parameter regions and instead truncate curves in some figures at longer stipe lengths. This procedure accounts for the apparently incomplete lines that appear in some panels.

Effects of plant size

For both *Eisenia* and *Pterygophora*, increases in stipe length cause greater bending moments to be applied to the plants. These torque values increase rapidly as the seaweeds get taller and rise fastest in shallower water (Figs 5A, 6A). This trend is similar across wave height. Across the 0.1–2.0 m size range, *Pterygophora* is exposed to maximal bending moments approximately 1.5 times as large as those imposed on *Eisenia*.

The tensile stresses that arise from these bending moments also generally increase with increasing stipe length, although much less drastically than for bending moment. In one case (*Eisenia* growing at deeper depths for H=2 m; Fig. 5Bi), an increase from moderate to large size actually leads to a slight reduction in stress. In all other cases, longer stipes induce greater maximal stresses for plants located at a given depth and exposed to a given wave height. Of the two species, *Pterygophora* experiences substantially larger stresses than *Eisenia*. This difference is almost a factor of five, and is more or less constant across depth and wave height.

Effects of water depth

Plants of a given species universally experience greater bending moments and tensile stresses in shallower water (Figs 5, 6). This trend is most pronounced for larger plants, but is similar across wave heights despite the difference in absolute magnitude of bending moment or stress. In general, the model predicts that stresses in 18 m of water are approximately half of those in 6 m of water. Note that the shallowest depth (3 m) shown for H=2 m (Figs 5, 6, column i) is not presented for the two larger wave heights (Figs 5, 6, columns ii, iii) because of the constraint on H due to the depth at which waves break.

Effects of wave height

Larger wave height produces larger bending moments and tensile stresses. This trend is strongest for plants with longer stipes (Figs 5, 6).

Effects of wave period

In contrast to L, d and H, wave period plays only a minor role in affecting bending moment or stress. This result follows from the fact that horizontal velocities are largely independent of wave period in water depths less than approximately 25 m for periods greater than approximately 7 s (Kinsman, 1965). As a consequence, we include no figures related to τ.

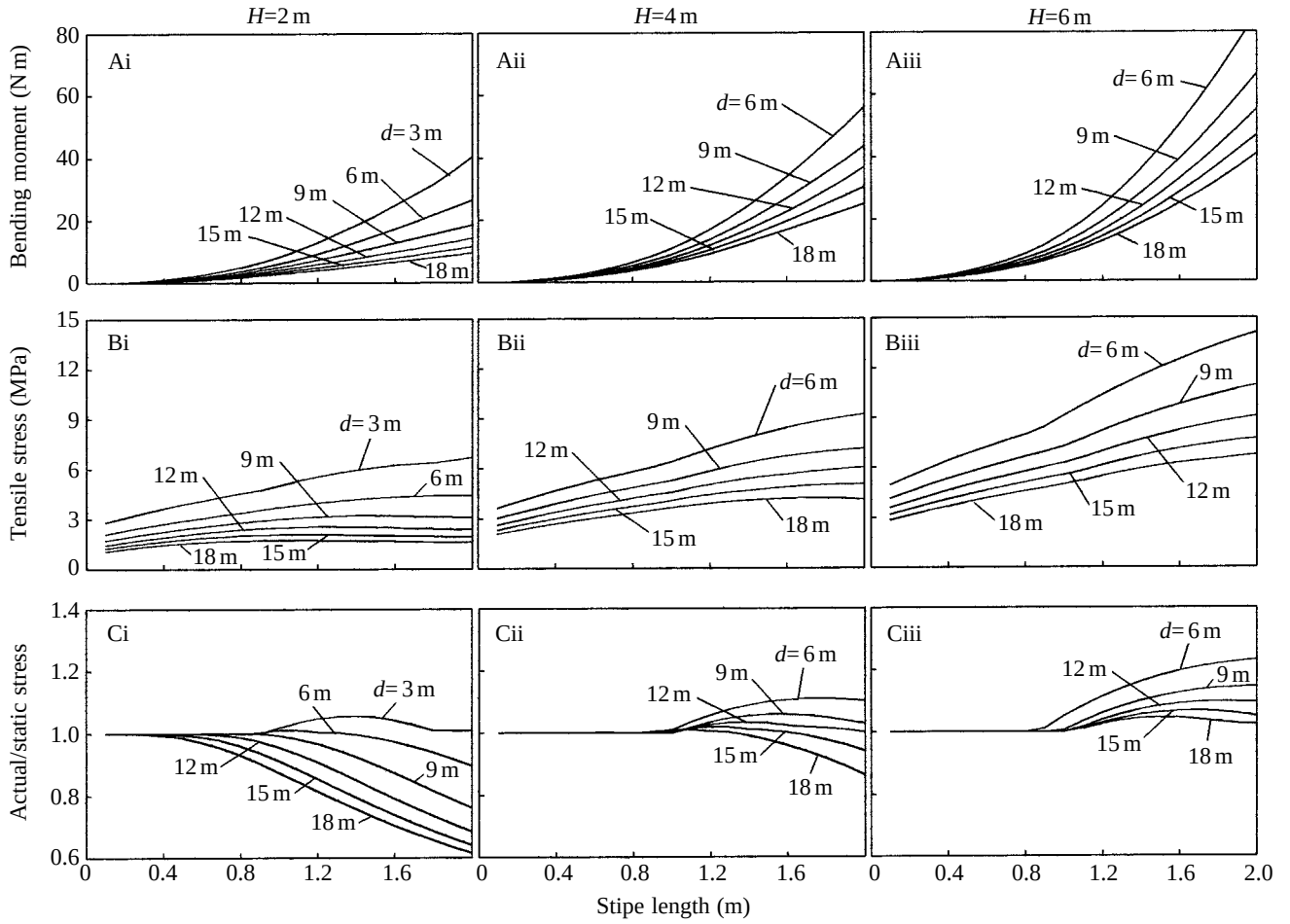

Fig. 5. Numerical model results for allometrically growing *Eisenia arborea*. (A) Bending moments, (B) tensile stresses and (C) stress ratios across a range of stipe lengths, *L*, and water depths, *d*. Wave height, *H*, is 2 m (Ai,Bi,Ci), 4 m (Aii,Bii,Cii) or 6 m (Aiii,Biii,Ciii). The wave period is 10 s.

Effects of plant shape

Isometric 'small-shape' growth (isometric growth with the L=0.1 m plant morphology) leads to much greater bending moments and stresses at large plant size than those that arise from the measured allometric growth patterns (Figs 7, 8). This is true for both species. For example, small-shape isometric growth would induce bending moments in large *Eisenia* living in 6 m of water that are nearly 50 times those found from the normal allometric growth curves. Similarly, bending moments acting on large *Pterygophora* plants at this same depth would be nearly 25 times higher in the small-shape isometric case. Peak stresses in small-shaped plants would be approximately 1.5 times as large in *Eisenia* and 2–3.5 times greater in *Pterygophora*. In contrast to the small-shape isometric growth forms, the 'large-shape' isometric growth curves (isometric growth with the adult L=2 m plant form) are predicted to have little effect on stresses induced in the plants. The minor differences that do arise occur primarily at short stipe lengths where stresses are low. We therefore do not plot stress curves corresponding to the large-shape isometric patterns since they are nearly indistinguishable from the allometric results.

Effects of stipe stiffness

Increasing both the tensile and compressive moduli by a factor of 10 increases stresses substantially in both species. The opposite is true when the modulus is reduced by a factor of 10. Figs 9 and 10 show the ratio of the stresses that would result from a given change in tensile and compressive moduli (termed the 'altered stress') to the stresses predicted to arise in plants having normal modulus values. Data for a single wave height and period only are shown, but the trends are consistent across wave parameters.

Unequal tensile and compressive moduli also affects stresses. A modulus ratio (E_t/E_c) larger than 1 results in greater tensile stresses, but lower compressive stresses, than those generated in plants with equal tensile and compressive moduli. This topic will be addressed in further detail in the Discussion.

Effects of plant movement

The motion of the plants also modifies the level of stress they must endure. This effect can be seen in Figs 5C and 6C, which show the ratio of the maximum actual stresses felt by plants to the 'static' stresses they would feel if they simply

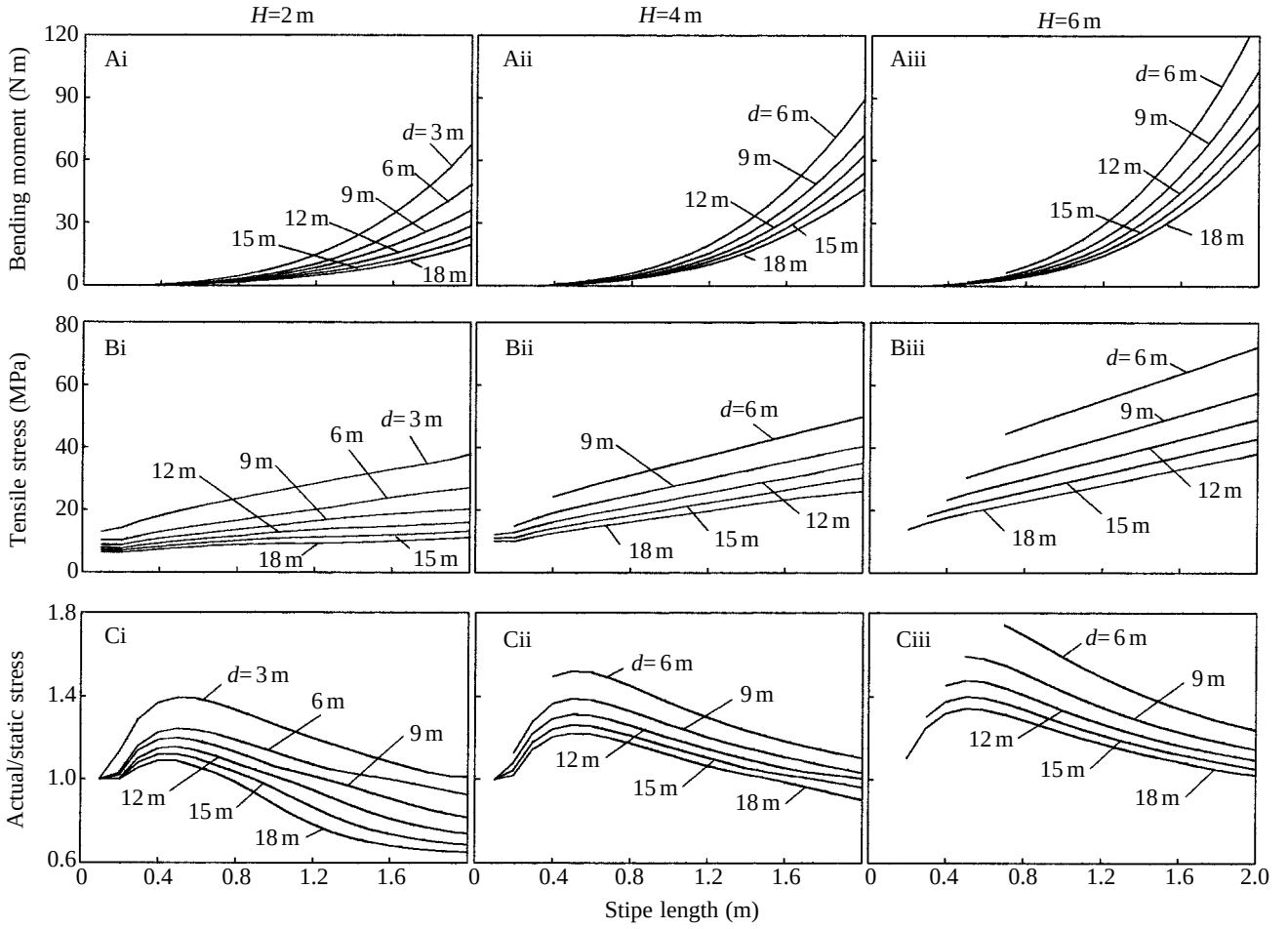

Fig. 6. Numerical model results for allometrically growing *Pterygophora californica*. (A) Bending moments, (B) tensile stresses and (C) stress ratios across a range of stipe lengths, *L*, and water depths, *d*. Wave height, *H*, is 2 m (Ai,Bi,Ci), 4 m (Aii,Bii,Cii) or 6 m (Aiii,Biii,Ciii). The wave period is 10 s.

came to static equilibrium with the largest hydrodynamic force imposed on them. The exact consequences of movement, however, depend critically on the species, plant size, water depth and wave height.

In *Eisenia* (Fig. 5C), there appears to be a threshold effect of size. Plants with stipes less than 1.0 m long experience stresses nearly identical to the static stress. In contrast, plants taller than 1.0 m show actual/static stress ratios that may be substantially lower, or somewhat higher, than unity, depending on water depth and wave height. In general, large seaweeds of this species experience stress amelioration under small waves owing to dynamic effects, but feel stress exacerbation under large waves.

In contrast to *Eisenia*, the actual/static stress curves for *Pterygophora* may deviate from 1 across essentially the full size range (Fig. 6C). The largest actual/static stress ratios tend to occur for plants with stipes approximately 0.5 m in length. For plants near this size growing in 6 m of water and exposed to 6 m waves, actual stresses may exceed static values by nearly a factor of 2. For plants living in deeper waters (d=15–18 m), there is less stress exacerbation for the small and mid-sized plants (L=0.1–0.7 m), and there may be substantial stress reduction at larger sizes (L>1.5 m) if the wave height is small (H=2 m). In general, however, the ratios of actual/static stress for large *Pterygophora* individuals are greater than 1 and are substantially higher than those predicted for *Eisenia*.

Discussion

Consequences of allometric growth

In both *Eisenia* and *Pterygophora*, growth according to the measured allometric relationships is predicted to reduce stresses greatly, particularly at large sizes, relative to those that would arise if the plants were to grow isometrically with their ‘small’ shapes. This suggests that allometric growth may be an important factor allowing these kelps to reach the upper end of their observed size ranges. The lower stresses follow from the fact that the allometry of both *Eisenia* and *Pterygophora* reflects a change in plant form from a high-drag to a lower-drag morphology as size increases. That is, taller *Eisenia* and *Pterygophora* individuals typically support less blade material for their size than do shorter organisms. Note that, although

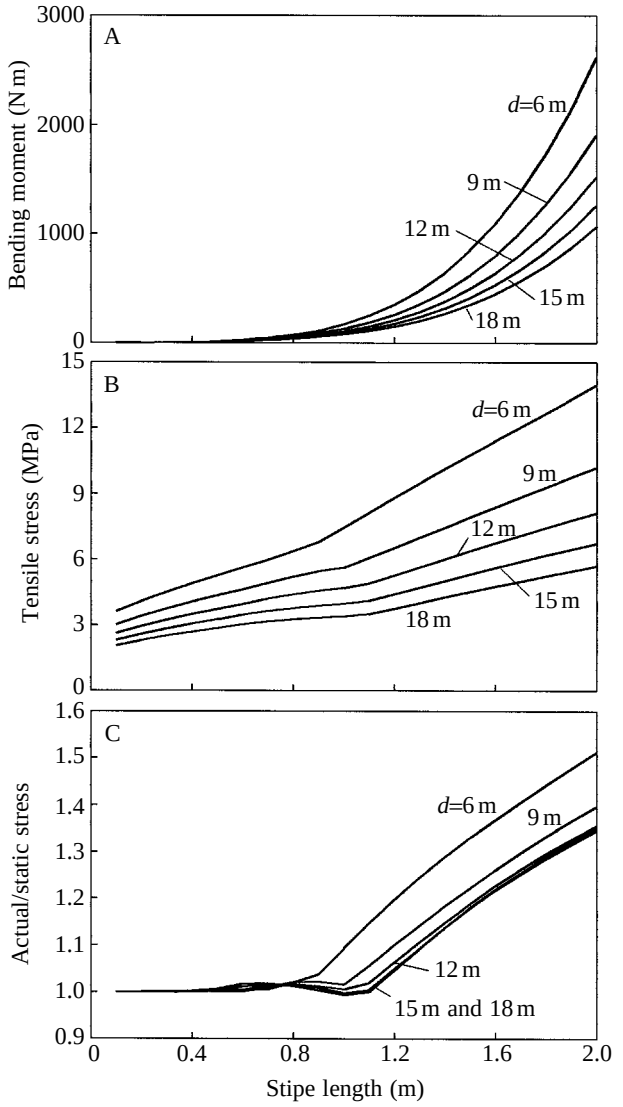

Fig. 7. Numerical model results for *Eisenia arborea* growing isometrically according to its 'small' shape (see text). (A) Bending moment, (B) tensile stress and (C) stress ratio as a function of stipe length. Data are for multiple depths (*d*), but fixed wave height (4 m) and wave period (10 s).

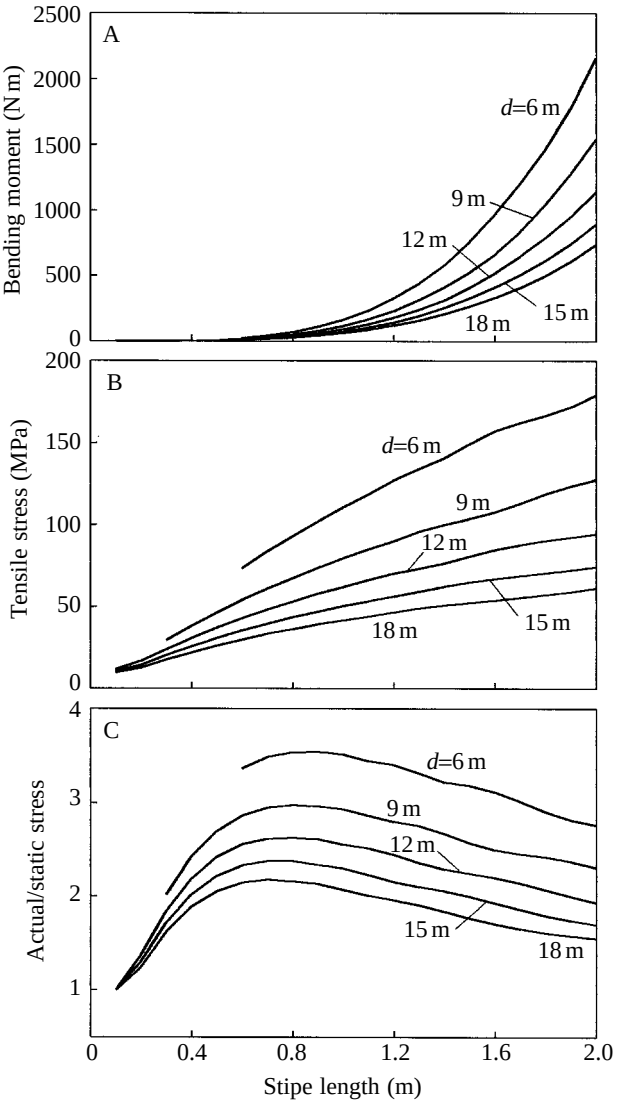

Fig. 8. Numerical model results for *Pterygophora californica* growing isometrically according to its 'small' shape (see text). (A) Bending moment, (B) tensile stress and (C) stress ratio as a function of stipe length. Data are for multiple depths (*d*), but fixed wave height (4 m) and wave period (10 s).

'large'-shape isometric growth would produce stresses no greater than those predicted for the allometric case, such growth patterns would lead to plants with less relative blade area at small sizes. This could reduce photosynthetic capacity and growth rates in juveniles, making them more susceptible to overshading and competition early in life and reducing survivorship.

Previously, Neushul (1972) noted the difficulty in distinguishing between exceptionally young individuals of the various species of stipitate kelps and has proposed that this may reflect hydrodynamic constraints on the juvenile form. However, the fact that stresses in small organisms are predicted by the present model to be universally low, regardless of growth mode, suggests that fluid-mechanical bounds (if they indeed exist) operate more plausibly at large than at small plant sizes.

Scaling arguments have often been applied to explain why organisms change shape with growth. For example, McMahon (1973) has shown that a variety of terrestrial organisms scale according to the principle of 'elastic similarity', whereby deflections (normalized to length) remain invariant across size. He shows that for elastically similar structures loaded in bending principally by their own weight (i.e. for dense structures in air) and undergoing small deflections, radius increases with length raised to the power 3/2. This relationship, however, does not apply to nearly neutrally buoyant organisms such as kelp, where the dominant bending forces scale more closely with area (*via*

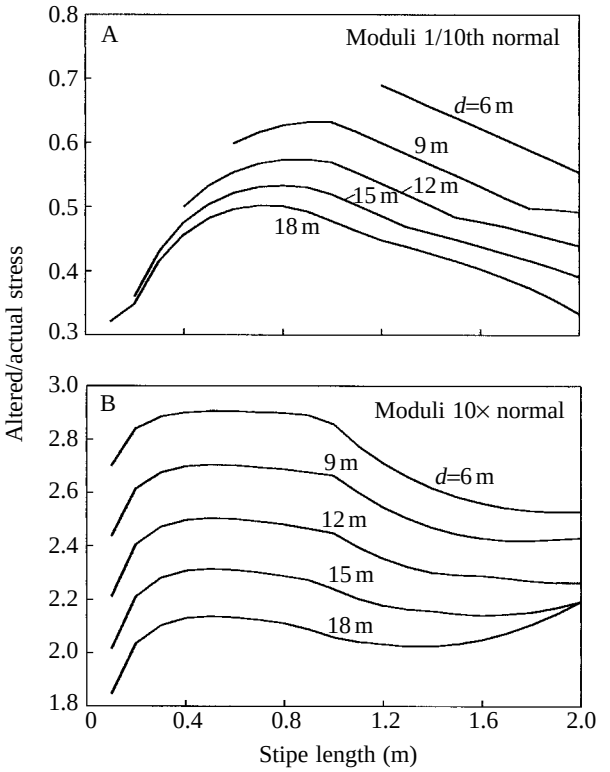

Fig. 9. Ratio of the stresses that would occur if the moduli of allometrically growing *Eisenia arborea* were (A) 1/10th or (B) 10 times the normal stresses that are predicted to occur in this species. Data are presented as a function of stipe length and water depth (*d*) for fixed wave height (4 m) and wave period (10 s).

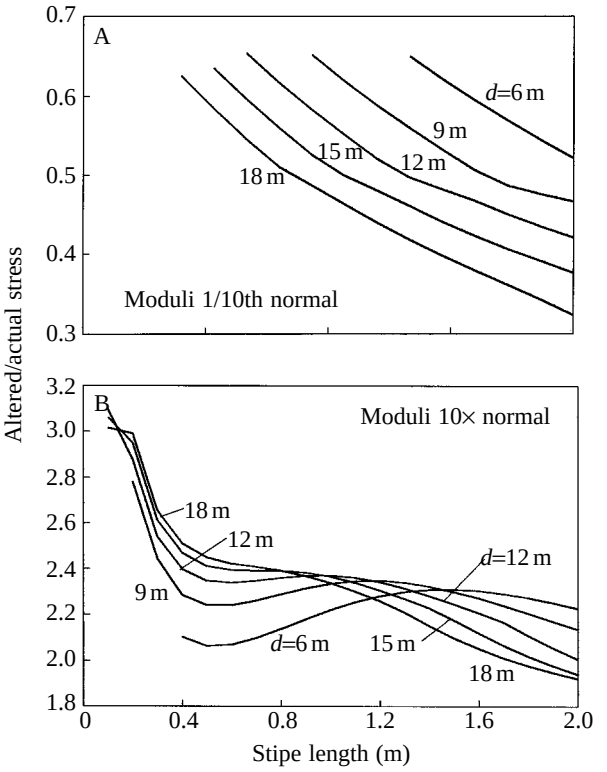

Fig. 10. Ratio of the stresses that would occur if the moduli of allometrically growing *Pterygophora californica* were (A) 1/10th or (B) 10 times the normal stresses that are predicted to occur in this species. Data are presented as a function of stipe length and water depth (*d*) for fixed wave height (4 m) and wave period (10 s).

drag; equation 13) than with weight. Under these conditions, the elastic similarity criterion implies instead a three-way relationship among radius, length and area:

$$r^4 \propto AL^2 . \qquad (25)$$

This relationship can be derived by substituting A (as an index of the magnitude of drag) for F in equation 4, and noting that the moment of inertia scales with radius raised to the fourth power. It might also be mentioned that if A is assumed to scale with L^2 and radius varies linearly with length, then an elastically similar structure in bending will also show 'stress similarity', whereby peak stresses remain identical across size (the criterion for this, from equation 12, is that $r^3 \propto AL$). For *Eisenia* and *Pterygophora*, the allometric data of Table 3 suggest that neither species shows elastic similarity and, of the two, only *Pterygophora* might be expected to demonstrate stress similarity. However, such simple scaling arguments ignore dynamics, nonlinearities associated with large deflections and variations in moduli and flow regime with size. When these factors are considered *via* the numerical model, the results indicate that *Pterygophora* in no way shows the stress similarity one might expect from elementary analyses. This is apparent from this species' increase in stress with L in Fig. 6B.

Material property effects

Increases in moduli with size

The rapid rise in material stiffness with increasing stipe length observed for both *Eisenia* and *Pterygophora* (Table 3) counteracts some of the effects of their allometric changes in shape. For example, although the scaling of radius, area and length predict that deflections (relative to stipe length) should increase as the plants grow taller, the concomitant rise in E more than offsets this trend to produce normalized deflections that actually decrease as the kelps become larger. Some of the relative merits of larger or smaller deflections are discussed below.

Increasing or decreasing the moduli

As shown in Figs 9 and 10, a decrease in material stiffness (resulting in an increase in flexibility and greater deflections) effectively reduces stresses in both species. The lower stresses follow from the fact that a decrease in moduli allows the stipes of these seaweeds to bend farther in response to an applied load, decreasing the moment arm of the imposed force. We explore a portion of the physics of this process in Fig. 11, for the simplified situation where forces are applied as constant loads. Under such static conditions, shifting both moduli away from their original levels to new values, E'_t and E'_c, while

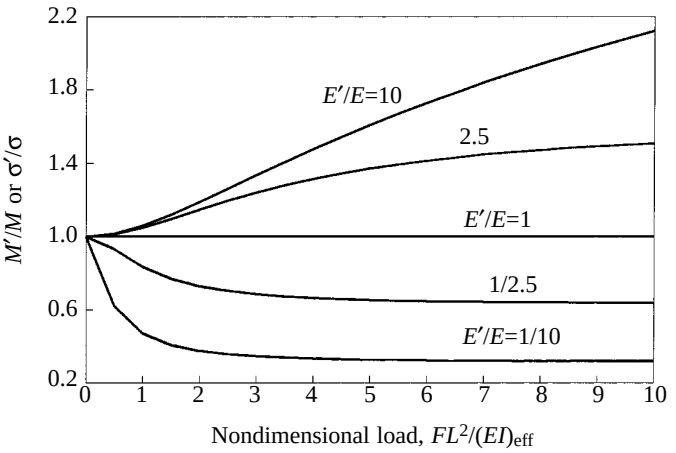

Fig. 11. Effect on static bending moment or stress of increasing or decreasing both moduli while holding the modulus ratio constant. E'/E denotes the ratio of the altered to the original modulus values and is identical for both the tensile and compressive moduli. M'/M is the ratio of the altered to the original moment, and σ'/σ is the ratio of the altered to the original stress. F, load; L, stipe length; $(EI)_{eff}$, effective flexural stiffness.

keeping the modulus ratio constant (i.e. $E'_t/E'_c=E_t/E_c$, where E_t and E_c are the original values) can have a substantial effect on the magnitude of the new maximal bending moment (M') imposed. The change in bending moment, in turn, affects the new stress (σ') in an identical fashion. For example, decreasing both moduli by a factor of 10 lowers the bending moment and stress by approximately 70 %, relative to the values (M or σ, respectively) that would result from applying the same force to a stipe possessing the original moduli. In contrast, a 10-fold increase in moduli produces bending moments that rise rapidly with increasing nondimensionalized load, $FL^2/(EI)_{eff}$, to a value more than double that for the original moduli at $FL^2/(EI)_{eff}=10$. Here, $(EI)_{eff}$ is the effective flexural stiffness of the beam computed using the original moduli. These relationships account for most of the patterns seen in Figs 9 and 10. Although the curves of Fig. 11 are functions of the nondimensionalized force, they are independent of both the original moduli and the modulus ratio *per se* (i.e. they are functions only of $E'/E\equiv E'_t/E_t=E'_c/E_c$). Note that a given shift in stiffness affects both the tensile and compressive stresses in an identical manner.

The low-modulus effects detailed in the lower curves of Fig. 11 are the primary reason that *Eisenia* is predicted to experience relatively smaller stresses than *Pterygophora*. Note, however, that allometry (in particular the thick stipe and lower blade area) also plays a role in the smaller stresses of *Eisenia*. Even if the moduli of this alga were increased by a factor of 10, it would still experience stresses only approximately half as large as those induced in *Pterygophora*.

Unequal moduli

Having unequal moduli in tension and compression also strongly influences the bending moments and stresses acting on the stipes of these species. In particular, ratios of E_t/E_c greater than 1 result in higher tensile stresses, but lower compressive stresses, than if the moduli were identical. The opposite is true for modulus ratios less than 1. Such stress modification arises from the interplay of three linked factors. Recall from equations 10 and 11 that the tensile or compressive bending stress in a stipe is a function of $\bar{y}_t$ or $\bar{y}_c$, $(EI)_{eff}$ and M. Varying the ratio E_t/E_c affects all of these quantities by shifting the location of the neutral axis. We discuss the way in which this occurs for each factor in turn.

The location of the neutral axis is set by the requirement that a cross section of a non-moving beam in bending must be in static equilibrium (see Appendix). As a consequence, a stipe with a lower compressive than tensile modulus has a neutral surface that is shifted towards the tensile side of the stipe. In contrast, a stipe with higher compressive than tensile stiffness has its neutral surface shifted towards the compressive side. This directly affects the magnitude of $\bar{y}_t$ or $\bar{y}_c$, as shown in Fig. 12. The distance from the neutral axis to the tensile surface of a stipe cross section declines as the ratio E_t/E_c increases, while the distance from the neutral axis to the compressive surface shows the opposite trend.

The change in the effective stiffness of a stipe can be evaluated in either of two ways. If the departure of the modulus ratio away from unity is viewed as resulting from a (developmental or evolutionary) shift of a plant's tensile modulus away from an original modulus, $\hat{E}$ (i.e. $E_c=\hat{E}$), then the effective stiffness rises for $E_t/E_c>1$ and declines for $E_t/E_c<1$. In contrast, the opposite holds if E_t remains constant

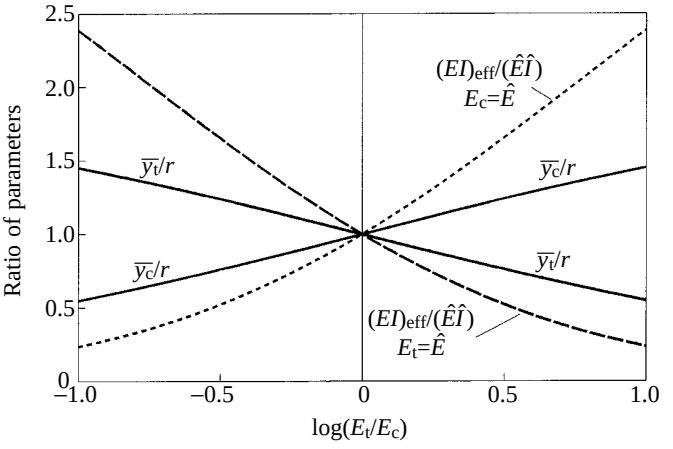

Fig. 12. Shift in the location of the neutral axis and effective flexural stiffness that follows from having unequal moduli ($E_t/E_c\neq1$). $\bar{y}_t/r$ and $\bar{y}_c/r$ are the distances of the neutral axis from the tensile or compressive sides of the stipe, respectively, divided by the stipe radius, r. The long-dashed line is the effective flexural stiffness curve, $(EI)_{eff}/(\hat{E}\hat{I})$, and corresponds to the case where the compressive modulus is decreased relative to an invariant tensile modulus (i.e. $E_t=\hat{E}$), while the short-dashed line is the effective stiffness curve representing an increase in tensile modulus relative to a constant compressive modulus (i.e. $E_c=\hat{E}$). $\hat{E}\hat{I}$ is the effective flexural stiffness computed when $E_t=E_c=\hat{E}$.

and E_c varies. Both of these lines are shown in Fig. 12, where values of the effective stiffness are plotted relative to a 'default' effective stiffness, $\hat{E}\hat{I}$, calculated for the condition where both moduli are equal to $\hat{E}$.

Movement of the neutral axis away from the center of the stipe also alters the nonlinear geometry of the deflected stipe by causing it to bend to a different position for a given load. Thus, the bending moment, M, is modified *via* a change in the length of the moment arm (L–δ_{axl}) of the applied force. However, unlike the location of the neutral axis and the value of the effective stiffness, which depend only on the modulus ratio (E_t/E_c) and the value of the original modulus ($\hat{E}$), the bending moment acting on a stipe also depends on the magnitude of the applied force. If E_t is varied (i.e. $E_c=\hat{E}$), then the magnitude of the bending moment (M) increases as E_t/E_c rises (Fig. 13A). Alternatively, if E_c varies relative to a fixed modulus of $E_t=\hat{E}$, then M declines as the modulus ratio gets larger (Fig. 13B). Under both conditions, the change in the bending moment increases as the applied load increases. For generality, M is shown relative to the moment that would arise if the stipe's moduli were equal ($\hat{M}$), and the force is nondimensionalized as $FL^2/(\hat{E}\hat{I})$.

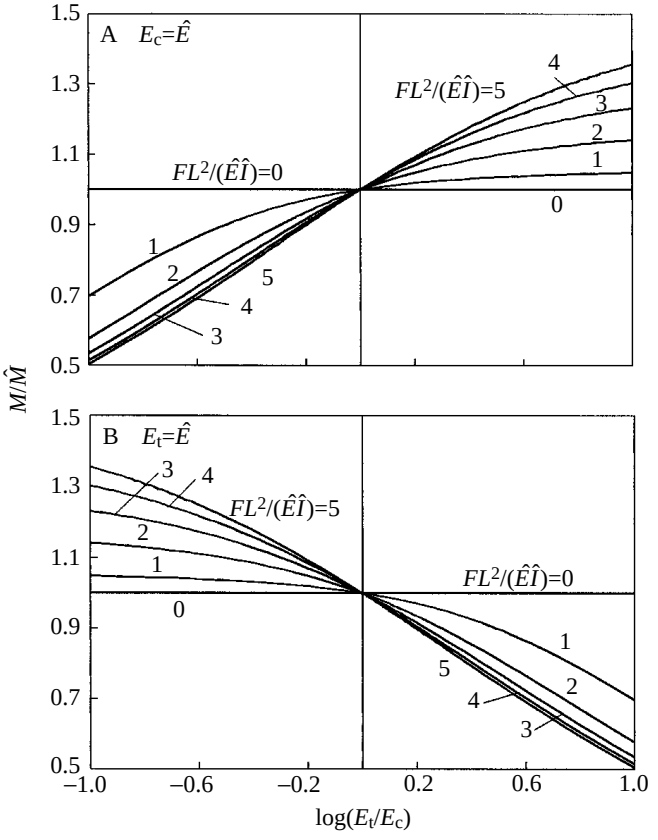

Fig. 13. Effects on the bending moment of having unequal moduli as a function of the nondimensionalized force, $FL^2/(\hat{E}\hat{I})$. Bending moments increase with larger E_t/E_c ratios for $E_c=\hat{E}$ (A) or decrease for larger E_t/E_c (B) if $E_t=\hat{E}$. $\hat{M}$ and $\hat{E}\hat{I}$ are the bending moment and effective flexural stiffness, respectively, computed when $E_t=E_c=\hat{E}$. $M/\hat{M}$ is the ratio of the altered to the original moment.

The overall effect of non-equal tensile and compressive moduli on stresses induced in a stipe can therefore be expressed as the product of the three factors discussed above multiplied by a ratio reflecting the magnitude of the tensile or compressive modulus relative to $\hat{E}$.

$$\frac{\sigma_t}{\hat{\sigma}} = \left(\frac{M}{\hat{M}}\right)\left(\frac{\bar{y}_t}{r}\right)\left(\frac{\hat{E}\hat{I}}{(EI)_{eff}}\right)\left(\frac{E_t}{\hat{E}}\right), \quad (26)$$

$$\frac{\sigma_c}{\hat{\sigma}} = \left(\frac{M}{\hat{M}}\right)\left(\frac{\bar{y}_c}{r}\right)\left(\frac{\hat{E}\hat{I}}{(EI)_{eff}}\right)\left(\frac{E_c}{\hat{E}}\right), \quad (27)$$

where $\hat{\sigma}$ is the maximum stress that would occur in a stipe of equivalent geometry if both moduli were equal to $\hat{E}$.

We consider first the case of tensile stress. As noted above, the first term in equation 26 either increases or decreases with increasing E_t/E_c. It can also be either greater or less than unity, depending on whether the tensile or compressive modulus is varied. The second term always decreases as the modulus ratio rises. The product of the third and fourth terms rises rapidly with increasing E_t/E_c and plays a dominant role in the equation. The consequences of the combination of these three linked effects can be seen in Fig. 14. If the tensile modulus is varied relative to a fixed value of $E_c=\hat{E}$, then tensile stresses rise as the modulus ratio increases (Fig. 14A). This trend is more marked for larger forces. A similar pattern results for the case where E_c is varied in relation to $E_t=\hat{E}$ (Fig. 14B). However, in this situation, the greatest stress ratios occur for smaller forces. The net result for *Eisenia* and *Pterygophora*, which have $E_t/E_c>1$, is that, regardless of which modulus varies, tensile stresses are always larger than they would be if E_t and E_c were equal. Unfortunately, Biedka *et al.* (1987) considered the role only of the second term of equation 26 when they proposed that an E_t/E_c ratio greater than 1 decreases tensile stresses.

Analogous patterns arise for the compressive stresses (indeed, note the considerable symmetry between Figs 14 and 15). As in equation 26, the first term of equation 27 can be either greater or less than 1. The second term now increases with increasing E_t/E_c, however, while the product of the third and fourth terms drops sharply as the modulus ratio gets larger. These effects result in compressive stress ratios that decrease as E_t/E_c increases. For an altered tensile modulus relative to an invariant compressive modulus ($E_c=\hat{E}$), the stress ratios deviate farthest from unity for small forces (Fig. 15A). The contrary is true for a constant tensile modulus with variable E_c (Fig. 15B). Because $E_t/E_c>1$ for both *Eisenia* and *Pterygophora*, these plants therefore experience much lower compressive stresses in their stipes than they would if both moduli were equal.

Note that, while we show explicitly the consequences of varying only one modulus value at a time (i.e. either E_t or E_c is always held constant), the data of Figs 12 and 13 can be used to explore the effects of shifts in modulus of any sort *via* iterative multiplication of the appropriate ratios.

As noted cursorily in the Results, the maximum ratio of tensile to compressive stress itself is a constant also set by the

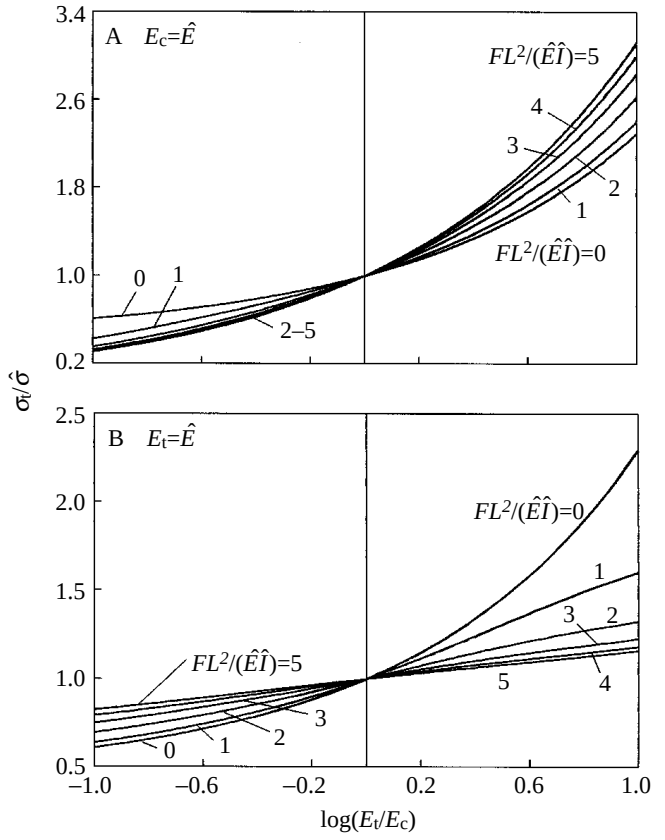

Fig. 14. Effects on the tensile stress of having unequal moduli, as a function of the nondimensionalized force, $FL^2/(\hat{E}\hat{I})$. Tensile stresses rise with larger E_t/E_c ratios either for $E_c=\hat{E}$ (A) or for $E_t=\hat{E}$ (B). $\hat{\sigma}$ and $\hat{E}\hat{I}$ are the tensile stress and effective flexural stiffness, respectively, computed when $E_t=E_c=\hat{E}$. $\sigma/\hat{\sigma}$ is the ratio of the altered to the original stress.

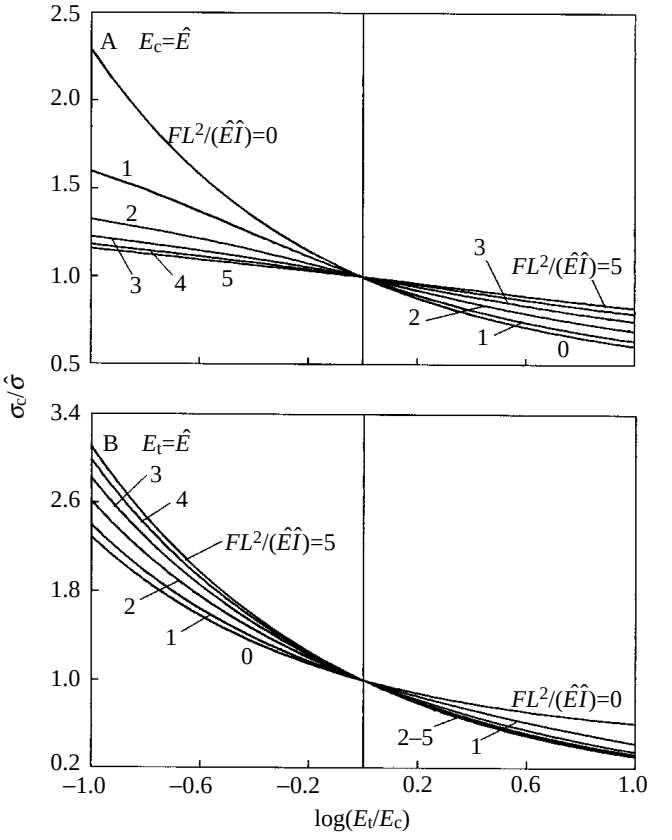

Fig. 15. Effects on the compressive stress of having unequal moduli, as a function of the nondimensionalized force, $FL^2/(\hat{E}\hat{I})$. Compressive stresses decline with larger E_t/E_c ratios either for $E_c=\hat{E}$ (A) or for $E_t=\hat{E}$ (B). $\hat{\sigma}$ and $\hat{E}\hat{I}$ are the tensile stress and effective flexural stiffness, respectively, computed when $E_t=E_c=\hat{E}$. $\sigma/\hat{\sigma}$ is the ratio of the altered to the original stress.

ratio E_t/E_c. This can be seen by dividing equation 26 by equation 27, yielding:

$$\frac{\sigma_t}{\sigma_c}=\frac{\bar{y}_t E_t}{\bar{y}_c E_c}\ , \qquad (28)$$

and by noting (Fig. 12) that $\bar{y}_t/r$ and $\bar{y}_c/r$ are functions only of the modulus ratio. Since $\bar{y}_t E_t/\bar{y}_c E_c$ equals 1.92 for *Eisenia* and 2.45 for *Pterygophora* (Table 4), this explains why both species experience much higher tensile than compressive stresses.

The stipitate species tested in the present study are not the only members of the Laminariales that possess elastic moduli that are different in tension and in compression. Holbrook *et al.* (1991) report an E_t/E_c value of 2.97 for *Postelsia palmaeformis*, the 'sea palm', a species also characterized by an exceptionally flexible, cantilever-style stipe. E_t/E_c ratios greater than 1 may therefore be typical of plants within this algal order, as may the low stiffness that apparently exists as a concomitant trend. On a more perplexing note, however, Holbrook *et al.* (1991) also report estimates of 'bending modulus' that are higher than both their compressive and tensile measurements. This is unexpected: estimates from simple bending tests should produce values that fall intermediate to the actual tensile or compressive values if the moduli are substantially different. The tensile tests reported by Holbrook *et al.* (1991), however, were completed using excised tissue samples from plants collected from Tatoosh Island off the coast of Washington State, while compressive and bending experiments were performed using lengths of intact stipe from organisms collected in central California. These differences in preparation technique and/or population characteristics may provide one possible explanation. Theoretical considerations indicate that the hollow geometry typical of *Postelsia* stipes cannot itself account for the discrepancy.

The fact that all the stipitate kelps tested to date possess moduli that are apparently stiffer in tension than in compression suggests that there may be developmental, physical or environmental restrictions placed on the stipe material properties of these organisms. Currently, it is impossible to distinguish among these (or other) alternatives. We can, however, envision at least two biomechanical scenarios where it might be advantageous to have moduli like those of these plants. In the first case, the unequal moduli of

the stipes of these species are assumed to be an unavoidable consequence of their phylogeny, or the way in which their stipes are constructed. Tensile stresses are also assumed to be the most critical factor affecting the breakage of the stipes of these organisms. In this situation, the low moduli of *Eisenia* and *Pterygophora* could act as an effective survivorship-enhancing trait, largely ameliorating the consequences of the larger tensile stresses that arise when $E_t/E_c>1$ (see Figs 9–11). Alternatively, although most materials do indeed fail in tension, it is possible that the stipes of stipitate kelps are typically weakest in compression. In this scenario, low overall stiffness may act synergistically with an E_t/E_c ratio greater than 1 to reduce substantially the compressive stresses generated in the stipes of these plants (albeit at the expense of elevating tensile stresses). While this possibility remains purely conjectural at present, there is some suggestion that the stipes of *Eisenia* and *Pterygophora* may in fact be vulnerable to compressive failure. Preliminary experiments were conducted where severe bending loads were applied to the stipes of these species, first in one direction and then in the opposite direction. Often, a stipe could be bent to a particular deflection in the first direction without breaking, but then failed in tension when torqued to the identical deflection the other way. This suggests that compressive tissue damage to the stipe occurred in response to the first bending load, making the stipe susceptible to subsequent tensile failure at the damaged location when the force was reversed.

Importance of dynamics

Material property effects are further complicated in flexible organisms by the plant movement that inexorably accompanies low stiffness. Such motion can introduce yet another factor modulating the levels of stresses induced in the stipes of stipitate kelps (Koehl, 1982, 1984, 1986; Koew and Wainwright, 1977).

For example, Koehl and co-workers have suggested that flexible organisms can reduce the forces felt from wave-driven water motion by 'going with the flow', reducing fluid velocities relative to themselves. Output from the present model supports this hypothesis, but suggests that going with the flow may be an effective stress-reducing mechanism only for some species of certain morphology growing in particular locations. In general, the model predicts that going with the flow is effective primarily only for plants longer than approximately 1 m, living at depths greater than approximately 10 m under waves less than 2 m high. Under these conditions, plants of this size are typically longer than the diameter of wave-driven water orbits and are unlikely to be bent to large deflections before the direction of water motion reverses. Since shorter plants cannot reorient during as large a fraction of the wave cycle, this strategy is less effective for them.

Going with the flow is also likely to be less beneficial in shallow water or under larger waves. As depth declines or wave height increases, the maximum horizontal excursion of the water orbits greatly increases, as does the magnitude of the water velocities themselves. Thus, not only does it become more difficult for a flexible organism to reorient through the entire wave cycle (i.e. the plant would have to be quite long, in principle), but the higher flows impose larger hydrodynamic forces. These larger forces tend to accelerate the mass of the organism itself to substantial velocity, giving it nontrivial momentum. Then, even as the flow declines, this momentum continues to carry the plant's mass in the direction in which it was originally pushed. Our numerical model suggests that this inertial effect can, in certain cases, cause plant stipes to bend farther than they would if the plants were allowed to reach equilibrium with the peak forces impinging on them. This especially appears to be the case for *Pterygophora* individuals of intermediate stipe length.

Note also that the potential for excessive swaying which accompanies low stiffness may at some point offset the stress-reducing benefits outlined in Figs 9 and 10. Kinematic data from computer analyses with moduli of 1/10th normal suggest that plants may swing to positions where most of the length of their stipes would lie parallel to the bottom and where much of the blade mass of the plants would strike the substratum with some regularity. This could increase an organism's susceptibility to damage from pounding and abrasion against the substratum. It is also possible that higher levels of dynamic swaying could increase the rate at which the blades themselves are torn, tattered and broken, similar to the way that the end of a snapped towel quickly frays.

Biological importance of wave action

Unfortunately, existing data on the breaking strength of algal materials is sparse. DeWreede *et al.* (1992) stretched tissue excised from the stipes of *Eisenia arborea* and *Pterygophora californica*, recording tensile breaking strengths of 6.0 and 6.6 MPa, respectively. It is unclear whether their experiments were completed on multiple stipes or multiple samples from single stipes of these species. Biedka *et al.* (1987) tested the material properties of tissue extracted from two *P. californica* stipes and report tensile breaking strengths between 5.7 and 9.2 MPa depending on tissue orientation. Neither of these studies explored potential variation in strength with plant size. There are apparently no data on compressive strength in these species.

Despite the paucity of strength measurements, the present study nevertheless suggests that wave forces may be important agents of dislodgment for understory kelps. Tensile stresses in the stipes of *Eisenia* are predicted by our model to approach or exceed the tensile breaking strength for this species (taken to be 6.0 MPa here) under certain conditions. The predictions for *Pterygophora* are even more striking; tensile stresses are universally, and for some plant sizes and wave conditions substantially, in excess of the expected stipe tensile breaking strength (also taken to be 6.0 MPa). This result at first appears disconcerting but, with further consideration, points to what may be another critically important feature of the structure of stipitate kelps that may allow them to survive more effectively the hydrodynamic forces imposed on them.

We propose that flexibility within the holdfasts of these kelps may be a key stress-reducing trait, acting synergistically

with the stress-mitigating effects of high stipe flexibility. The bending theory used in our model implicitly assumes that the base of a stipe is firmly and rigidly clamped in place and cannot move. This is a simplification. In practice, the stipes of both *Eisenia* and *Pterygophora* are held to the rock substratum by a flexible network of haptera, which allows the base of the stipes of these organisms to rotate slightly. Even a small amount of such reorientation can significantly reduce the curvature (and therefore the stress; see equations 1, 10 and 11) generated at the base of a bent stipe, where the stresses are largest. Thus, although the stresses predicted by our model to occur in the stipes of these seaweeds are probably overestimates, our predictions also suggest that, were it not for their flexible construction, *Eisenia* and *Pterygophora* might find it difficult to survive in the habitats where they do indeed live. Note that this stress amelioration occurs as a consequence of a reduction in curvature rather than from a significant decrease in the applied (as opposed to the internally induced) moment at the base of the stipe and, therefore, it does not (nor would it be expected to) disturb the close correspondence observed between the results of the field test and the numerical predictions.

Of the two species tested, *Eisenia* is predicted to experience much lower stresses across all plant sizes and water depths than *Pterygophora*, suggesting a reduced vulnerability to wave action. Indeed, the ability of *Eisenia* to resist severe flows effectively can be seen in the field data of Dayton *et al.* (1992), where survivorship of this species at 15 m depth following even the exceptional 1988 storm in southern California (see Seymour *et al.* 1989; Dayton *et al.* 1989) was 92 %. These high survival rates are remarkable considering the exceptionally large waves associated with this particular storm event.

In comparison, *Pterygophora* may be relatively more susceptible to the rigours of wave action. The model results suggest that stresses in *Pterygophora* stipes are almost five times greater than in *Eisenia*, while its breaking strength is approximately the same. We might therefore predict that the largest individuals of this species could survive only at relatively deeper (or more protected) sites than *Eisenia*, but we have not tested this expectation. Alternatively, *Pterygophora* may be able partially to circumvent the largest flow forces by reducing its blade area prior to the occurrence of winter storms since the sporophylls of this species become senescent and are lost in late autumn.

We emphasize, however, that, although our model and the data of Dayton *et al.* (1992) both suggest relative differences in the vulnerability of *Eisenia* and *Pterygophora* to wave action, marine macroalgae are notoriously morphologically plastic (e.g. Norton, 1969; Gerard, 1987; Kraemer and Chapman, 1991), with plant form and mechanical properties often correlated with the level of wave exposure (e.g. Gerard and Mann, 1979; Norton *et al.* 1981; Cousens, 1982; Koehl and Alberte, 1988; Jackelman and Bolton, 1990; Gutierrez and Fernandez, 1992; Johnson and Koehl, 1994). Such deviations in allometric growth patterns have the potential to modify strongly the susceptibility of kelps to severe flows.

We also note that stipe bending stresses and breaking strengths *per se* may not, at times, be the most important factors limiting persistence in these species. On the contrary, often the weakest link in the ability of these stipitate algae to resist wave-driven forces is the adhesion of the holdfast. For example, of 113 *Pterygophora californica* individuals washed up on the shore near Point Joe (Pebble Beach, California) following the first winter storm of 1994–95, 76 % had broken at the stipe while the rest had failed at the rock/holdfast interface. This suggests that substantial numbers of plants may be dislodged even by hydrodynamic forces insufficient to break stipes outright.

Biological factors may also have synergistic effects that couple with those associated with wave climate. Denny *et al.* (1989) and Biedka *et al.* (1987) have noted that algae are often composed of brittle (although highly extensible) materials. These sorts of materials typically fail abruptly once some critical level of stress is reached. This mode of failure is highly sensitive to surface imperfections or damage, particularly sharp-tipped nicks or cracks. Sea urchins of the genus *Strongylocentrotus* are notorious grazers on *Pterygophora* (Pearse and Hines, 1979; Watanabe and Harrold, 1991) and leave scars that can potentially make the stipe vulnerable to breakage from brittle fracture (Biedka *et al.* 1987; but see DeWreede *et al.* 1992). In some cases, such grazing effects can be important agents of damage or mortality (Koehl and Wainwright, 1977; Santelices *et al.* 1980; Tegner *et al.* 1995). Of the 113 *Pterygophora* we examined on the shore near Point Joe, many had stipes that had been grazed by amphipods, although the precise number was not quantified.

In addition to hydrodynamic forces and grazing, competition for light may also play a critical role in the survival of understory kelps. Watanabe *et al.* (1992) showed that photosynthesis and growth of *Pterygophora californica* can be inhibited by a dense surface canopy of *Macrocystis pyrifera* and note that, although *Pterygophora* commonly grows in relatively exposed locations where patches of surface canopy are periodically torn away, it tends not to be found in sheltered locations where the canopy remains intact throughout much of the year.

The persistence of understory stipitate kelps can furthermore be affected by their dynamic motion in ways other than those associated just with mechanical stresses and breakage. For example, the movement resulting from a plant's high flexibility allows stipitate seaweeds to bend to postures where their blades may sweep the substratum. Velimirov and Griffiths (1979) and Ojeda and Santelices (1984) suggest that this behavior might keep herbivores and competitors at bay.

Limitations of the model

The most severe simplification in the model is the absence of a vertically directed force balance to complement the horizontal equation of motion. This prevents consideration of the hydrodynamic forces arising from the vertical component of wave motion, as well as ignoring any vertical inertia of the plant itself. Although neither of these neglected factors is likely

to be of consequence, except for cases when inertially driven tip deflections become large, under these conditions, vertical inertia may become a non-trivial component of the dynamics of the system. This follows from the fact that, at large deflections when the algae are bent far over, their tips may be moving mostly either in an upward or downward direction. Unfortunately, a two-dimensional model that incorporates both horizontal and vertical force balances is computationally intensive and suffers from mathematical asymptotic difficulties for some loading conditions. Note that, although vertical forces are neglected, the vertical attenuation of velocities with depth and the distance of the tip of the stipe from the substratum are considered in the model.

The manner in which we have modeled drag acting on these organisms is also a simplification. With γ less than 2 (equation 13), drag coefficients decline with velocity and therefore appropriately represent the reconfiguration of blade bundles that occurs in these organisms in response to changes in velocity magnitude. The drag equation we have used, however, is less effective in accounting for the directional reorientation and resulting 'slack' configurations that occur with long blades when the flow reverses. Including features to account for such reorientation behavior in the model is a natural place to focus subsequent efforts. Potential variation in drag coefficient with plant size might be explored as well.

We have also ignored torsion (twisting), the distributed hydrodynamic forces acting on the stipe and any taper [and thus changes in $(EI)_{\mathrm{eff}}$] along the length of the stipe. Torsion may be important where small-scale topography disturbs the two-dimensionality of the local flow or where geometric asymmetries of the organisms themselves are positioned obliquely to the oncoming waves. Given the substantially larger projected blade area compared with stipe area, and the relatively low degree of taper observed in most individuals of the two species, distributed forces and a variable effective flexural stiffness are unlikely to affect the conclusions of the model materially. We also used only circular stipe cross sections (as opposed to elliptical) in the model since, in general, there was only moderate deviation from circularity (except distally where stipe curvature becomes small) and because the orientation and degree of eccentricity were inconsistent from plant to plant.

The model we have employed also assumes that the materials from which the stipes are constructed are perfectly elastic and homogeneous, show no hysteresis and have stiffnesses that do not depend directly on strain rate or the magnitude of strain. Although such features may be important, a full exploration of their effects awaits further tests of material properties in these organisms.

We have also neglected higher-order terms in the expression we have used to model the added mass force in our equation of motion. However, these terms [which arise as a result of spatial gradients in fluid velocity (Miloh, 1994)] are probably negligible for the flow conditions typically encountered by stipitate kelps.

We emphasize that, despite the above simplifications, we feel that the model accounts for the dominant physical factors experienced by these stipitate organisms in flow and provides a first quantitative (although approximate) estimate of the behavior of these biological structures in response to time-varying fluid forces. The close match between the model predictions and the field measurements lends further support to this view. Three major points emerge from this study. First, *Eisenia arborea* and *Pterygophora californica* appear to grow according to allometric plans that result in internal stresses that are much reduced compared with isometric growth with a juvenile shape. This allometry may enhance the growth potential of juvenile sizes while reducing the risks of dislodgment from wave action in larger plants. Second, the model shows that flexibility provides an effective means of reducing the stresses generated in the tissues of these organisms by allowing the plants to bend and shorten the moment arms of the applied forces. This effect interacts with the additional stress-modifying consequences of having a higher tensile than compressive modulus. Third, the numerical model demonstrates that the dynamic motion that follows from the great flexibility of these plants results (under certain conditions) in either stress reduction or increases in stress. These deviations in stress from static values can at times be considerable.

Appendix

Location of the neutral axis in an elliptical cross section

Conditions of static equilibrium dictate that there is no net force acting on the cross section of a beam in bending. Thus:

$$\int_{\mathrm{Tensile}} \sigma_t \mathrm{d}A_t + \int_{\mathrm{Compressive}} \sigma_c \mathrm{d}A_c = 0 \,, \qquad \text{(A1)}$$

where A_t is the tensile area of the cross section of a bent beam and A_c is the compresssive area of the cross section of a bent beam, and the two integrals are evaluated over the tensile and compressive regions of the cross section, respectively.

Since:

$$\sigma_t = -E_t \kappa \bar{y} \quad \text{and} \quad \sigma_c = -E_c \kappa \bar{y} \,, \qquad \text{(A2)}$$

where $\bar{y}$ denotes the distance from the neutral axis, combining equations A1 and A2 yields:

$$E_t \int_{\mathrm{Tensile}} \bar{y} \mathrm{d}A_t + E_c \int_{\mathrm{Compressive}} \bar{y} \mathrm{d}A_c = 0 \,. \qquad \text{(A3)}$$

The equation of an ellipse is:

$$\frac{X^2}{r_1^2} + \frac{Y^2}{r_2^2} = 1 \,. \qquad \text{(A4)}$$

Thus, in the case of an elliptical cross section with semi-axes r_1 and r_2 (r_2 in the plane of bending), equation A3 becomes:

$$E_t \int_{y_n}^{r_2} 2\frac{r_1}{r_2}(Y - y_n)\sqrt{(r_2^2 - Y^2)}\mathrm{d}Y = E_c \int_{-r_2}^{y_n} 2\frac{r_1}{r_2}(Y - y_n)\sqrt{(r_2^2 - Y^2)}\mathrm{d}Y \,, \qquad \text{(A5)}$$

where y_n is the distance of the neutral axis from the centroidal

axis of the beam. Utilizing the change of variable $\sin\psi = Y/r_2$ and carrying out the integration produces the relationship:

$$(E_t - E_c)\left(\frac{(r_2^2 - y_n^2)^{3/2}}{3} + \frac{y_n r_2^2}{2}\arcsin\frac{y_n}{r_2} + \frac{y_n^2}{2}\sqrt{(r_2^2 - y_n^2)}\right) - (E_t + E_c)\frac{y_n r_2^2 \pi}{4} = 0 . \quad \text{(A6)}$$

Equation A6 is then solved iteratively for y_n.

Effective flexural stiffness of a beam with an elliptical cross section

Noting that the applied external moment equals the total moment produced by the internal stresses acting over the cross section:

$$M = \int \sigma \bar{y} dA = \int_{\text{Tensile}} \sigma_t \bar{y} dA_t + \int_{\text{Compressive}} \sigma_c \bar{y} dA_c . \quad \text{(A7)}$$

Substituting from equations A2:

$$M = -\kappa E_t \int_{\text{Tensile}} \bar{y}^2 dA_t - \kappa E_c \int_{\text{Compressive}} \bar{y}^2 dA_c , \quad \text{(A8)}$$

where the integrations are carried out over the tensile and compressive regions of the cross section, respectively. Noting that:

$$I_t = \int_{\text{Tensile}} \bar{y}^2 dA_t \qquad I_c = \int_{\text{Compressive}} \bar{y}^2 dA_c \quad \text{(A9)}$$

and substituting yields:

$$M = -\kappa(E_t I_t + E_c I_c) . \quad \text{(A10)}$$

Comparison with equation 1 shows that the term in parentheses can thus be considered the 'effective' flexural stiffness of the beam, $(EI)_{\text{eff}}$. Using equation A4 for an ellipse and substituting into equations A9 produces:

$$I_t = \int_{y_n}^{r_2} 2\frac{r_1}{r_2}(Y - y_n)^2 \sqrt{(r_2^2 - Y^2)} dY$$

$$I_c = \int_{-r_2}^{y_n} 2\frac{r_1}{r_2}(Y - y_n)^2 \sqrt{(r_2^2 - Y^2)} dY . \quad \text{(A11)}$$

Integrating by parts once, using the substitution $\sin\psi = Y/r_2$ and then integrating by parts again gives:

$$I_t = 2\frac{r_1}{r_2}\left\{-\left[\frac{y_n^2 r_2^2}{2}\arcsin\frac{y_n}{r_2} + \frac{3y_n^3}{4}\sqrt{(r_2^2 - y_n^2)} + \frac{2y_n}{3}(r_2^2 - y_n^2)^{3/2} + \frac{r_2^4}{8}\arcsin\frac{y_n}{r_2} - \frac{r_2^2 y_n}{8}\sqrt{(r_2^2 - y_n^2)}\right] + \left[\frac{y_n^2 r_2^2 \pi}{4} + \frac{r_2^4 \pi}{16}\right]\right\} \quad \text{(A12)}$$

$$I_c = 2\frac{r_1}{r_2}\left\{\left[\frac{y_n^2 r_2^2}{2}\arcsin\frac{y_n}{r_2} + \frac{3y_n^3}{4}\sqrt{(r_2^2 - y_n^2)} + \frac{2y_n}{3}(r_2^2 - y_n^2)^{3/2} + \frac{r_2^4}{8}\arcsin\frac{y_n}{r_2} - \frac{r_2^2 y_n}{8}\sqrt{(r_2^2 - y_n^2)}\right] + \left[\frac{y_n^2 r_2^2 \pi}{4} + \frac{r_2^4 \pi}{16}\right]\right\} . \quad \text{(A13)}$$

These values of I_t and I_c are then used in equation A10 to find $(EI)_{\text{eff}}$.

We thank J. Leichter, L. Roberson, B. Hale, D. Stokes and G. Villa for field assistance. This study was funded by NSF grants OCE 91-15688 and OCE 93-13891 to M.W.D.

References

ABBOTT, I. A. AND HOLLENBERG, G. J. (1976). *Marine Algae of California*. Stanford, CA: Stanford University Press.

ABRAMOWITZ, M. AND STEGUN, I. A. (1965). *Handbook of Mathematical Functions*. New York: Dover Publications, Inc.

BATCHELOR, G. K. (1967). *An Introduction to Fluid Dynamics*. Cambridge, UK: Cambridge University Press.

BELL, E. C. AND GOSLINE, J. M. (1996). Mechanical design of mussel byssus: material yield enhances attachment strength. *J. exp. Biol.* **199**, 1005–1017.

BIEDKA, R. F., GOSLINE, J. M. AND DEWREEDE, R. E. (1987). Biomechanical analysis of wave-induced mortality in the marine alga *Pterygophora californica*. *Mar. Ecol. Prog. Ser.* **36**, 163–170.

CARRINGTON, E. (1990). Drag and dislodgment of an intertidal macroalga: consequences of mophological variation in *Mastocarpus papillatus* Kutzing. *J. exp. mar. Biol. Ecol.* **139**, 185–200.

CHARTERS, A. C., NEUSHUL, M. AND BARILOTTI, C. (1969). The functional morphology of *Eisenia arborea*. *Proc. int. Seaweed Symp.* **6**, 89–105.

COUSENS, R. (1982). The effect of exposure to wave action on the morphology and pigmentation of *Ascophyllum nodosum* (L.) Le Jolis in south-eastern Canada. *Bot. mar.* **25**, 191–195.

DANIEL, T. L. (1984). Unsteady aspects of aquatic locomotion. *Am. Zool.* **24**, 121–134.

DAYTON, P. K., SEYMOUR, R. J., PARNELL, P. E. AND TEGNER, M. J. (1989). Unusual marine erosion in San Diego County from a single storm. *Est. Coast Shelf Sci.* **29**, 151–160.

DAYTON, P. K., TEGNER, M. J., PARNELL, P. E. AND EDWARDS, P. B. (1992). Temporal and spatial patters of disturbance and recovery in a kelp forest community. *Ecol. Monogr.* **62**, 421–445.

DENNY, M. W. (1988). *Biology and the Mechanics of the Wave-swept Environment*. Princeton, NJ: Princeton University Press.

DENNY, M. W. (1995). Predicting physical disturbance: mechanistic approaches to the study of survivorship on wave-swept shores. *Ecol. Monogr.* **65**, 371–419.

DENNY, M. W., BROWN, V., CARRINGTON, E., KRAEMER, G. AND

MILLER, A. (1989). Fracture mechanics and the survival of wave-swept macroalgae. *J. exp. mar. Biol. Ecol*. **127**, 211–228.

DENNY, M. W., DANIEL, T. L. AND KOEHL, M. A. R. (1985). Mechanical limits to size in wave-swept organisms. *Ecol. Monogr*. **55**, 69–102.

DENNY, M. W. AND GAYLORD, B. (1996). Why the urchin lost its spines: hydrodynamic forces and survivorship in three echinoids. *J. exp. Biol*. **199**, 717–729.

DENNY, M. W., GAYLORD, B. AND COWEN, E. A. (1997). Flow and flexibiity. II. The role of size and shape in determining wave forces on the bull kelp *Nereocystis luetkeana*. *J. exp. Biol*. **200**, 3165–3183.

DEWREEDE, R. E., EWANCHUK, P. AND SHAUGHNESSEY, F. (1992). Wounding, healing and survivorship in three kelp species. *Mar. Ecol. Prog. Ser*. **82**, 259–266.

ECKART, C. (1952). The propagation of waves from deep to shallow water. In *Gravity Waves*, Circular no. **521**, pp. 165–173. National Bureau of Standards.

EMSON, R. H. AND FALLER-FRITSCH, R. J. (1976). An experimental investigation into the effect of crevice availability on abundance and size-structure in a population of *Littorina rudis* (Maton): Gastropoda: Prosobranchia. *J. exp. mar. Biol. Ecol*. **23**, 285–297.

GAYLORD, B., BLANCHETTE, C. A. AND DENNY, M. W. (1994). Mechanical consequences of size in wave-swept algae. *Ecol. Monogr*. **64**, 287–313.

GERARD, V. A. (1987). Hydrodynamic streamlining of *Laminaria saccharina* Lamour. in response to mechanical stress. *J. exp. mar. Biol. Ecol*. **107**, 237–244.

GERARD, V. A. AND MANN, K. H. (1979). Growth and production of *Laminaria longicruris* (Phaeophyta) populations exposed to different intensities of water movement. *J. Phycol*. **15**, 33–41.

GERE, J. M. AND TIMOSHENKO, S. P. (1990). *Mechanics of Materials*, 3rd edn. Boston, MA: PWS-Kent Publishing Co.

GUBBAY, S. (1983). Compressive and adhesive strengths of a variety of British barnacles. *J. mar. biol. Ass. U.K*. **63**, 541–555.

GUTIERREZ, L. M. AND FERNANDEZ, C. (1992). Water motion and morphology in *Chondrus crispus* (Rhodophyta). *J. Phycol*. **28**, 156–162.

HOLBROOK, N. M., DENNY, M. W. AND KOEHL, M. A. R. (1991). Intertidal "trees": consequences of aggregation on the mechanical and photosynthetic properties of sea-palms *Postelsia palmaeformis* Ruprecht. *J. exp. mar. Biol. Ecol*. **146**, 39–67.

JACKELMAN, J. J. AND BOLTON, J. J. (1990). Form variation and productivity of an intertidal foliose *Gigartina* species (Rhodophyta) in relation to wave exposure. *Hydrobiologia* **204/205**, 57–64.

JOHNSON, A. S. AND KOEHL, M. A. R. (1994). Maintenance of dynamic strain similarity and environmental stress factor in different flow habitats: thallus allometry and material properties of a giant kelp. *J. exp. Biol*. **195**, 381–410.

KATZ, S. L. AND GOSLINE, J. M. (1994). Scaling modulus as a degree of freedom in the design of locust legs. *J. exp. Biol*. **187**, 207–223.

KINSMAN, B. (1965). *Wind Waves*. Englewood Cliffs, NJ: Prentice-Hall.

KOEHL, M. A. R. (1977). Effects of sea anemones on the flow forces they encounter. *J. exp. Biol*. **69**, 87–105.

KOEHL, M. A. R. (1982). The interaction of moving water and sessile organisms. *Scient. Am*. **247**, 124–132.

KOEHL, M. A. R. (1984). How do benthic organisms withstand moving water? *Am. Zool*. **24**, 57–70.

KOEHL, M. A. R. (1986). Seaweeds in moving water: form and mechanical function. In *On the Economy of Plant Form and Function* (ed. T. J. Givnish), pp. 603–634. Cambridge, UK: Cambridge University Press.

KOEHL, M. A. R. AND ALBERTE, R. S. (1988). Flow, flapping and photosynthesis of *Nereocystis luetkeana*: a functional comparison of undulate and flat blade morphologies. *Mar. Biol*. **99**, 435–444.

KOEHL, M. A. R. AND WAINWRIGHT, S. A. (1977). Mechanical adaptations of a giant kelp. *Limnol. Oceanogr*. **22**, 1067–1071.

KRAEMER, G. P. AND CHAPMAN, D. J. (1991). Biomechanics and alginic acid composition during hydrodynamic adaptation by *Egregia menziesii* (Phaeophyta) juveniles. *J. Phycol*. **27**, 47–53.

MCMAHON, T. A. (1973). Size and shape in biology. *Science* **179**, 1201–1204.

MENGE, B. A. (1978). Predation intensity in a rocky intertidal community. *Oecologia* **34**, 1–16.

MILOH, T. (1994). Pressure forces on deformable bodies in non-uniform inviscid flows. *Q. J. mech. appl. Math*. **47**, 635–661.

MURDOCK, G. R. AND CURREY, J. D. (1978). Strength and design of shells of the two ecologically distinct barnacles, *Balanus balanus* and *Semibalanus (Balanus) Balanoides* (Cirripedia). *Biol. Bull. mar. biol. Lab., Woods Hole* **155**, 169–192.

NEUSHUL, M. (1972). Functional interpretation of benthic marine algal morphology. In *Contributions to the Systematics of Benthic Marine Algae of the North Pacific* (ed. I. A. Abbott and M. Kurogi), pp. 47–53. Kobe, Japan: Japanese Society of Phycology.

NORTON, T. A. (1969). Growth form and environment in *Saccorhiza polyschides*. *J. mar. biol. Ass. U.K*. **49**, 1025–1045.

NORTON, T. A., MATHIESON, A. C. AND NEUSHUL, M. (1981). Morphology and environment. In *The Biology of Seaweeds* (ed. C. S. Lobban and M. J. Wynne), pp. 421–451. Berkeley, California: University of California Press.

OJEDA, F. P. AND SANTELICES, B. (1984). Ecological dominance of *Lessonia nigrescens* (Phaeophyta) in central Chile. *Mar. Ecol. Prog. Ser*. **19**, 83–91.

PEARSE, J. S. AND HINES, A. H. (1979). Expansion of a central California kelp forest following the mass mortality of sea urchins. *Mar. Biol*. **51**, 83–91.

PRESS, W. H., TEUKOLSKY, S. A., VETTERLING, W. T. AND FLANNERY, B. P. (1992). *Numerical Recipes*. Cambridge, UK: Cambridge University Press.

RICKETTS, E. F., CALVIN, J. AND HEDGPETH, D. W. (1985). *Between Pacific Tides*, 5th edn. Stanford, CA: Stanford University Press.

SANTELICES, B., CASTILLA, J. C. AND SCHMIEDE, C. (1980). Comparative ecology of *Lessonia nigrescens* and *Durvillaea antarctica* (Phaeophyta) in central Chile. *Mar. Biol*. **59**, 119–132.

SEYMOUR, R. J., TEGNER, M. J., DAYTON, P. K. AND PARNELL, P. E. (1989). Storm wave induced mortality of giant kelp, *Macrocystis pyrifera*, in southern California. *Est. Coast Shelf Sci*. **28**, 277–292.

SPRUGEL, D. G. (1983). Correcting for bias in log-transformed allometric equations. *Ecology* **64**, 209–210.

TEGNER, M. J., DAYTON, P. K., EDWARDS, P. B. AND RISER, K. L. (1995). Sea urchin cavitation of giant kelp (*Macrocystis pyrifera* C. Agardh) holdfasts and its effects on kelp mortality across a large California forest. *J. exp. mar. Biol. Ecol*. **191**, 83–99.

THOMSON, W. T. (1993). *Theory of Vibrations with Applications*, 4th edn. Englewood Cliffs, NJ: Prentice-Hall.

UTTER, B. D. AND DENNY, M. W. (1996). Wave induced forces on the giant kelp *Macrocystis pyrifera* (Agardh): field test of a computational model. *J. exp. Biol*. **199**, 2645–2654.

VELIMIROV, B. AND GRIFFITHS, C. L. (1979). Wave-induced kelp movement and its importance for community structure. *Bot. mar*. **22**, 169–172.

WAINWRIGHT, S. A., BIGGS, W. D., CURREY, J. D. AND GOSLINE, J. M. (1976). *Mechanical Design in Organisms*. London, UK: Edward Arnold.

WATANABE, J. M. AND HARROLD, C. (1991). Destructive grazing by sea urchins *Strongylocentrotus* spp. in a central California kelp forest: potential roles of recruitment, depth and predation. *Mar. Ecol. Prog. Ser.* **71**, 125–141.

WATANABE, J. M., PHILLIPS, R. E., ALLEN, N. H. AND ANDERSON, W. A. (1992). Physiological response of the stipitate understory kelp, *Pterygophora californica* Ruprecht, to shading by the giant kelp, *Macrocystis pyrifera*. *J. exp. mar. Biol. Ecol.* **159**, 237–252.

YULE, A. B. AND WALKER, G. (1987). Adhesion in barnacles. *In Crustacean Issues*, 5, *Barnacle Biology* (ed. A. J. Southward), pp. 389–402. Rotterdam, Netherlands: A. A. Balkeam.

ZAR, J. H. (1974). *Biostatistical Analysis*. Englewood Cliffs, NJ: Prentice-Hall.